RESEARCH ARTICLE

Key Points:
- Nuominhe high-MgO potassic basalts show less EM1 affinity than other potassic basalts in northeast China
- Melt-rock interaction contributed the high-MgO composition of Nuominhe basalts
- The extent of melt-rock interaction decreased temporally and Rb/Nb, Ba/Nb, K/La, and Ba/La increased

Supporting Information:
- Supporting Information S1
- Table S1
- Table S2
- Table S3

Correspondence to:
L.-H. Chen,
chenlh@nju.edu.cn

The role of melt-rock interaction in the formation of Quaternary high-MgO potassic basalt from the Greater Khingan Range, northeast China

Jian-Qiang Liu[1] [ID], Li-Hui Chen[1] [ID], Xiao-Jun Wang[1], Yuan Zhong[1], Xun Yu[1] [ID], Gang Zeng[1] [ID], and Saskia Erdmann[1] [ID]

[1]State Key Laboratory for Mineral Deposits Research, School of Earth Sciences and Engineering, Nanjing University, Nanjing, China

Abstract Melt-rock interaction between ascending melt and peridotite results in mantle metasomatism and also leads to compositional modification of the primary melt. While this process is known to occur, it is less well understood how the reactions and the composition of the resulting magma temporally evolve. Here whole-rock major and trace element, Sr-Nd-Pb-Hf isotopes, and olivine major element composition of Quaternary Nuominhe basalts in the Greater Khingan Range of northeast China are presented to unravel how melt-rock interaction modified the composition of the high-MgO potassic basalts as time progressed. The Nuominhe basalts are predominantly basanite with high MgO (8.1–16.8 wt %) and high total alkali content ($K_2O + Na_2O = 6.0$–9.2 wt %). They have high K_2O/Na_2O ratios ($K_2O/Na_2O = 0.77$–1.24) and low SiO_2 and Al_2O_3 content ($SiO_2 = 44.4$–48.7 wt %, $Al_2O_3 = 10.5$–13.2 wt %). They are characterized by enrichment in strongly incompatible elements, positive Ba, K, and Sr and negative Th, U, Zr, Hf, and Ti anomalies, similar to the composition of enriched mantle (EM1)-type oceanic island basalts (OIBs). Their isotopic composition also compares to that of EM1-type OIBs (i.e., with $^{87}Sr/^{86}Sr = 0.70467$–0.70483, $\varepsilon_{Nd} = -4.1$ to -1.5, $\varepsilon_{Hf} = -0.3$ to 2.3, $^{206}Pb/^{204}Pb = 17.03$–17.36). These elemental and isotopic characteristics are consistent with the interpretation that the potassium-rich melts were derived from recycled crustal materials with EM1 signature. Phlogopite-bearing mantle xenoliths and zoned olivine xenocrysts with high Fo_{89-92} and low CaO (<0.1 wt %) core and low Fo_{75-86} and high CaO (>0.1 wt %) rim composition record interaction between the ascending melt and mantle peridotite. Basalts erupted during late stages (Late Pleistocene and Holocene) of activity at the Nuominhe volcanic field show notably higher SiO_2 content, Rb/Nb, Ba/Nb, K/La, and Ba/La, and lower MgO content than early-stage basalts (Early and Middle Pleistocene), which we infer to reflect a temporally decreasing extent of melt-rock interaction. During early stages of melt ascent, a reaction zone between melt channels and unreacted peridotite formed; at later stages this reaction zone effectively sealed the ascending melt from further reaction, resulting in increasing Rb/Nb, Ba/Nb, K/La, and Ba/La signatures of the erupted lavas.

1. Introduction

Continental and oceanic basalt erupted in intraplate settings commonly displays large compositional diversity. The most important controls on the compositional diversity are inferred to be heterogeneous mantle sources with variable amounts of recycled crustal components and/or variable degrees of mantle partial melting [*Hofmann and White*, 1982; *McKenzie and O'Nions*, 1991; *Weaver*, 1991; *Hofmann*, 1997, 2003; *Sobolev et al.*, 2005, 2007; *Willbold and Stracke*, 2006, 2010; *Walter et al.*, 2008, 2011; *Stracke*, 2012]. In addition to source heterogeneity, interaction between mantle-derived melt and surrounding rocks during ascent may also contribute to the compositional diversity of the erupted magma [*Wagner and Grove*, 1998; *Xu et al.*, 2005; *Tang et al.*, 2006; *Lambart et al.*, 2012; *Mallik and Dasgupta*, 2012, 2013, 2014; *Søager et al.*, 2013; *Zeng et al.*, 2013; *Mallik et al.*, 2015; *Liu et al.*, 2016]. Interaction between asthenosphere-derived alkali-rich melt and refractory lithospheric mantle has, for example, been proposed to explain the high SiO_2 and Cr and low Al_2O_3 and CaO content, and the "kinked" REE patterns of Hawaiian [*Wagner and Grove*, 1998] and Datong [*Xu et al.*, 2005] tholeiitic basalt, reflecting the crystallization of olivine and the consumption of orthopyroxene in melt-rock reactions. Experimental studies have confirmed that reaction between a siliceous melt and peridotite produces silica-undersaturated alkali melts owing to the formation of orthopyroxene and/or garnet at the expense of olivine [*Mallik and Dasgupta*, 2012, 2013, 2014], where the degree of alkalinity and silica undersaturation of the resulting melt increase with increasing system CO_2 content [*Mallik and Dasgupta*,

2014]. Despite abundant evidence that melt-rock interaction occurs in the shallow mantle and contributes to the compositional diversity of intraplate basalt [*Xu et al.*, 2005; *Søager and Holm*, 2013; *Zeng et al.*, 2013; *Liu et al.*, 2016], it is still not well understood how these reactions and thus the erupted basalt compositions spatially and temporally evolve, which we do in this contribution.

The object of our study are late Cenozoic continental intraplate volcanic rocks, which are widespread in northeast China (Figure 1 [*Basu et al.*, 1991; *Zhang et al.*, 1995; *Liu et al.*, 2001; *Zou et al.*, 2003, 2008; *Chen et al.*, 2007; *Kuritani et al.*, 2009, 2011, 2013; *Ho et al.*, 2013; *Chu et al.*, 2013; *Sun et al.*, 2014; *Zhao et al.*, 2014; *Liu et al.*, 2015]). They are mainly exposed along the flanks of the Songliao basin with the Greater Khingan Range in the west, the Lesser Khingan Range in the north, and the Changbaishan mountains in the east [*Liu et al.*, 2001]. Based on their K_2O content, the basalts can be subdivided into ultrapotassic series ($K_2O > 3$ wt % and $K_2O/Na_2O > 2$), potassic series ($K_2O > 3$ wt % and $1 < K_2O/Na_2O < 2$), and sodic series volcanic rocks [*Zhang et al.*, 1995; *Ho et al.*, 2013; *Sun et al.*, 2014]. Geochemical studies have inferred EM1-like mantle sources for these ultrapotassic (Xiaogulihe [*Sun et al.*, 2014, 2015]) and potassic rocks (Wudalianchi-Erkeshan-Keluo [*Zhang et al.*, 1995, 2000; *Zou et al.*, 2003; *Choi et al.*, 2006; *Kuritani et al.*, 2013; *Chu et al.*, 2013]; Nuominhe [*Zhao et al.*, 2014]). However, it remains controversial (1) whether the enriched sources of the potassic (and ultrapotassic) magmas were located in the lithospheric mantle [*Zhang et al.*, 1995; *Zou et al.*, 2003; *Chu et al.*, 2013; *Sun et al.*, 2014, 2015; *Zhang et al.*, 2016] or in the asthenosphere [*Choi et al.*, 2006; *Kuritani et al.*, 2013; *Liu et al.*, 2016] and (2) whether the enriched components originated from recycled sediments [*Kuritani et al.*, 2013; *Sun et al.*, 2014, 2015] or ancient lower continental crust [*Chu et al.*, 2013; *Zhao et al.*, 2014]. Our previous studies have shown that $^{87}Sr/^{86}Sr$, K_2O/Na_2O, and Rb/Nb of the potassic rocks are well correlated and that they decrease with increasing lithospheric thickness below individual volcanic centers [*Liu et al.*, 2016]. This correlation is well explained by variable degrees of interaction between the primary potassic melts and a cold lithospheric mantle, where reaction efficacy enhanced with increasing lithospheric thickness [*Liu et al.*, 2016]. The Nuominhe volcanic rocks, which are underlain by the thickest lithosphere of all investigated potassic volcanic fields (Figure 1b), show the strongest geochemical evidence for melt-rock interaction. Furthermore, the Nuominhe basalts erupted from Early Pleistocene to Holocene times in four main eruptive episodes [*Fan et al.*, 2012]. Therefore, these rocks provide an ideal opportunity to study the temporal progression of melt-rock interaction and the resulting melt and magma compositional evolution.

Here we present comprehensive major and trace element and Sr-Nd-Pb isotopic data and the first Hf isotopic data, together with the major element composition of olivine phenocrysts for the basaltic lavas from Nuominhe volcanic field (NVF). We show that compositional variations of the Nuominhe basalts are related to their eruption ages, reflecting varying extents of melt-rock interaction in the lithospheric mantle.

2. Geological Background and Petrography

Tectonically, the Greater Khingan Range and the Songliao Basin belong to the Xing'an-Mongolia Orogenic Belt (XMOB) (Figure 1a). The XMOB lies in the eastern part of the Central Asian Orogenic Belt (CAOB), which is a Paleozoic Orogenic Belt more than 1500 km wide, which formed during subduction and collision between the North China Craton to the south and the Siberian Craton to the north [*Sengör et al.*, 1993; *Jahn et al.*, 2000]. Several significant events have contributed to the formation and tectonic evolution of the XMOB, including the final closure of the Paleo-Asian Ocean, the amalgamation of several microcontinental massifs (the Erguna, Xing'an, Songliao, and Jiamusi-Khanka massifs), and the subduction of the Paleo-Pafic Ocean [*Sengör et al.*, 1993; *Sengor and Natalin*, 1996; *Tang et al.*, 2014]. Regional geophysical studies have confirmed that the lithospheric thickness at the center of the Songliao Basin is about 80 km, and that the minimum crustal thickness beneath the basin is 31 km. The Greater Khingan Range, in contrast, has a thicker lithosphere (120 to >150 km) and crust (35–40 km) (Figure 1b [*Ma*, 1987; *Guo et al.*, 2014; *Tao et al.*, 2014]).

The NVF is located in the northern Greater Khingan Range, covering an area of about 600 km^2 (123°00'–124°15'E, 49°10'–50°00'N; Figure 1c). Based on K-Ar ages of basaltic glass (2.3–0.13 Ma), volcanic field characteristics, stratigraphy, and weathering degree, the NVF magmatism can be subdivided into four eruptive episodes: Early Pleistocene, Middle Pleistocene, Late Pleistocene, and Holocene volcanic rocks (Figure 1c [*Fan et al.*, 2012]). Lavas erupted in the Early Pleistocene, with K-Ar ages between 2.3 Ma and 0.76 Ma, are largely restricted to exposure along the Nuominhe river and the Kuile river valley. Basalt erupted in the Middle Pleistocene constitutes the main part of the Quaternary volcanic field, which forms abundant, well-preserved

pyroclastic cones and craters with K-Ar ages ranging from 0.71 Ma to 0.58 Ma. Late Pleistocene and Holocene volcanic rocks are found in the Bila river valley, where they form fresh lava flows and spectacular volcanoes. The spatial and temporal distribution of the basaltic volcanic rocks highlights that the Cenozoic volcanism of the NVF migrated from east to west [*Fan et al.*, 2012].

Thirty representative basalt samples from the NVF were studied in thin section and by whole-rock geochemistry. Their stratigraphy, lithology, and locality are shown in Table S1 in the supporting information and Figure 1c. The Nuominhe basalts are aphyric to moderately phyric (<10 vol % crystals), and they have a massive to vesicular structure. Clinopyroxene and plagioclase macrocrysts are rare with <1 vol % each. Macrocrysts are dominantly olivine including cognate phenocrysts (5%–7%) and xenocrysts (1%–3%) derived from disaggregated mantle peridotite xenoliths. The olivine phenocrysts are subhedral to euhedral and up to 0.5–1 mm in diameter (Figure S1a), many of which contain glassy melt inclusions and spinel. The olivine xenocrysts are typically 1–3 mm in size. They are characterized by kink bands, irregular to subround shape and up to ~200 μm wide rims with regular embayments and round to euhedral grain boundary segments (Figures S1b and 2). The transition from Mg-rich cores to Fe-rich rims is relatively abrupt over a width of <50 μm (Figures 2a and 2b). The cores have higher Fo and NiO contents and lower FeO, CaO, and MnO contents than the rims (Figures 2c–2f). The microgranular matrix of the basaltic rocks is made up of olivine, clinopyroxene, plagioclase, opaque minerals, and glass. Some of the Nuominhe basalts also contain abundant spinel-facies peridotite ($Ol_{45-65}Opx_{30-40}Cpx_{0-15}Sp_{0-10}$) and a few garnet-facies peridotite ($Ol_{40-55}Opx_{20-35}Cpx_{0-10}Grt_{5-25}$) xenoliths, which are mainly distributed in two volcanic cones: Banlashan and Xiaosifangshan [*Sui et al.*, 2012, 2014] (Figure 1b). These mantle xenoliths are mainly composed of harzburgite with minor lherzolite. Intergranular, fine-grained phlogopite is present in some of the garnet harzburgites, which is characterized by high K_2O (8.42–10.14 wt %) and TiO_2 (5.41–7.79 wt %) contents [*Sui et al.*, 2014].

3. Geochemical Results

The bulk-rock major and trace element and the Sr-Nd-Hf-Pb isotopic composition of the Quaternary basalts from the NVF are given in Table S2. Major element composition of their olivine macrocrysts is listed in Table S3. The analytical methods used above are summarized in the supporting information [*Kuritani and Nakamura*, 2002; *Yang et al.*, 2010; *Yu et al.*, 2015].

The Nuominhe basalts have low SiO_2 (44.41–48.71 wt %) concentration and high total alkali ($K_2O + Na_2O$ = 6.02–9.18 wt %) content, and they mainly classify as basanite and rarely as phonotephrite or trachy basalt [*Le Bas et al.*, 1986] (Figure 3a). They have relatively high K_2O content (2.89–4.40 wt %) and K_2O/Na_2O ratios (0.77–1.24), plotting close to the field of potassic rocks (Figure 3b). Moreover, the Nuominhe basalts have the highest MgO content (8.10–16.81 wt %) among the Cenozoic continental intraplate basalts in northeast China (Figure 4), and we therefore refer to them as high-MgO potassic basalt. Their Al_2O_3 content (10.52–13.18 wt %) correlates negatively and their Ni (128–532 ppm) and Cr (175–738 ppm) content correlates positively with MgO (Figures 4a, 4d, and S2c). The $Fe_2O_3^T$ (9.93–11.20 wt %) content of the Nuominhe rocks remains largely constant with decreasing MgO (Figure 4b). At MgO > 12 wt %, the CaO/Al_2O_3 ratios are invariant (Figure 4c). However, at MgO < 12 wt %, they decrease slightly with decreasing MgO, but their CaO/Al_2O_3 compositional range is relatively narrow (0.59–0.77), comparing with that of Cenozoic sodic basalts from northeast China (Figure 4c). In addition, the potassic (and ultrapotassic) basalt samples have low Al_2O_3 and high K_2O and P_2O_5 contents at a given MgO content compared to the Cenozoic sodic basalts (Figures 4a and S2a and S2b [see *Zhang et al.*, 1995; *Chu et al.*, 2013; *Sun et al.*, 2014]). Chondrite-normalized rare earth element (REE) patterns of the Nuominhe basalt reveal that they are enriched in light REEs over heavy REEs ((La/Yb)$_N$ = 29.74–48.0) with no Eu or Ce anomaly (Figure S3). In the primitive mantle-normalized incompatible trace element diagram, the Nuominhe high-MgO potassic basalt samples show positive Ba, K, and Sr anomalies and negative Th, U, Zr-Hf, and Ti anomalies, which are similar to those of the Wudalianchi-Erkeshan-Keluo potassic basalts, the Xiaogulihe ultrapotassic basalt, and the EM1 end-member (Figure 5) [*Chauvel et al.*, 1997].

The Nuominhe high-MgO potassic basalt samples exhibit a limited range in Sr, Nd, and Hf isotopic composition ($^{87}Sr/^{86}Sr$ = 0.704666–0.704833, ε_{Nd} = −4.1 to −1.5, ε_{Hf} = −0.28 to 2.26; Figures 6a and 6b). They are more enriched than mantle xenoliths entrained in the Keluo basalt [*Zhang et al.*, 2011] and other Cenozoic mantle xenoliths in eastern China (Figures 6a and 6b), but they are less enriched than the Wudalianchi-Erkeshan-Keluo potassic basalt and the Xiaogulihe ultrapotassic basalt (Figures 6a and 6b). The Nuominhe high-MgO
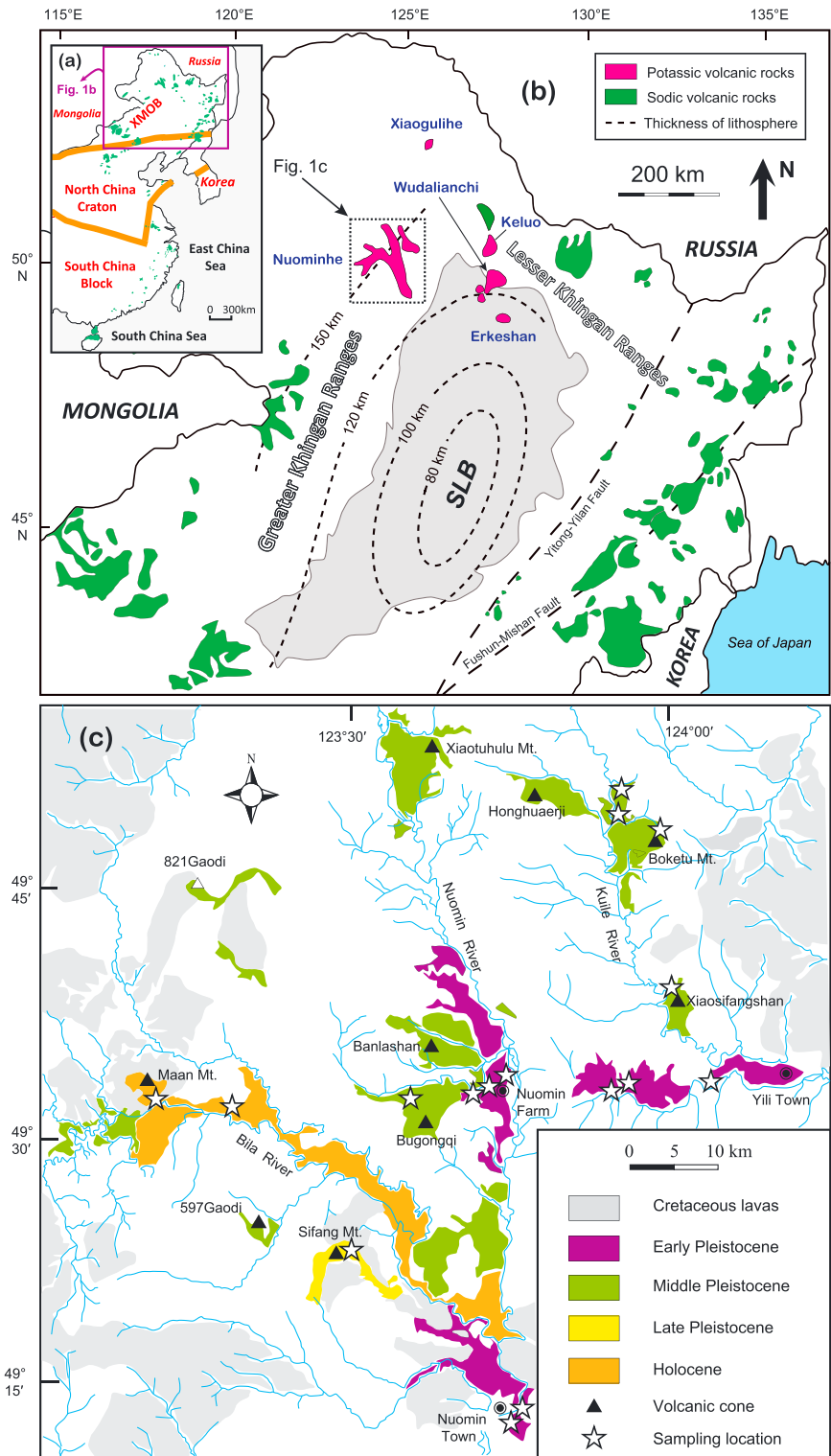
Figure 1. (a) Simplified geological map shows the spatial distribution of tectonic plates and Cenozoic volcanic rocks in eastern China. XMOB represents Xing'an-Mogolia Orogenic Belt. (b) Sketch geological map showing the distribution of Cenozoic volcanic rocks in northeast China (modified from *Liu et al.* [2001]). The contours represent estimated lithospheric thickness beneath the Songliao Basin and the Greater Khingan Range [*Ma*, 1987]. SLB means Songliao Basin. (c) Distribution and sampling locations for the Quaternary basalts of the Nuominhe volcanic field, Greater Khingan Range (modified after *Fan et al.* [2012]). Basalts are subdivided into four eruptive episodes according to their K-Ar ages: Early Pleistocene, Middle Pleistocene, Late Pleistocene, and Holocene [*Fan et al.*, 2012].
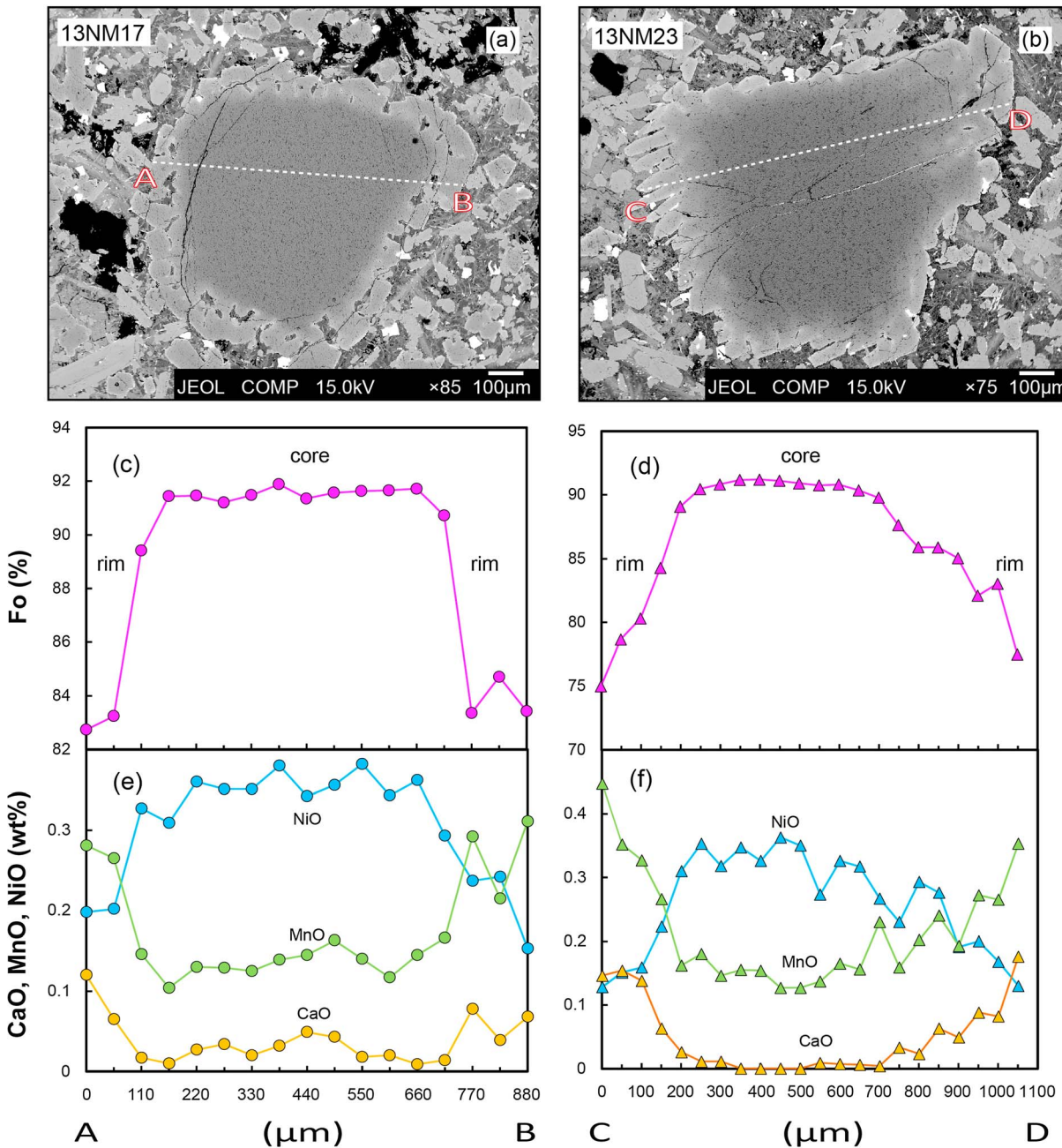
Figure 2. Core-rim compositions of two representative zoned olivine xenocrysts from samples 13NM17 and 13NM23 of the Nuominhe volcanic rocks. (a and b) Backscattered electron images show the compositional traverses (c–f) marked by white dotted lines. The cores have higher Fo and NiO and lower MnO and CaO content than the rims.

potassic basalt lavas also have a relatively homogeneous Pb isotopic composition (^{206}Pb/^{204}Pb = 17.030–17.364, ^{207}Pb/^{204}Pb = 15.416–15.460, ^{208}Pb/^{204}Pb = 37.057–37.480) (Table S3). In the ^{206}Pb/^{204}Pb-^{87}Sr/^{86}Sr and ^{206}Pb/^{204}Pb-ε_{Nd} isotopic correlation diagrams (Figures 6c and 6d), the Nuominhe high-MgO potassic basalt samples plot close to the EM1 end-member.

The analyzed olivine macrocrysts of the Nuominhe potassic basalts have a wide range of compositions (Table S3): Fo (75.8–92.4), MnO (0.032–0.371 wt %), NiO (0.132–0.435 wt %), and CaO (0.023–0.434 wt %). They can be subdivided into magmatic phenocrysts and fragmented mantle-derived xenocrysts based on their textures and compositions. The olivine phenocrysts are commonly subhedral to euhedral in texture
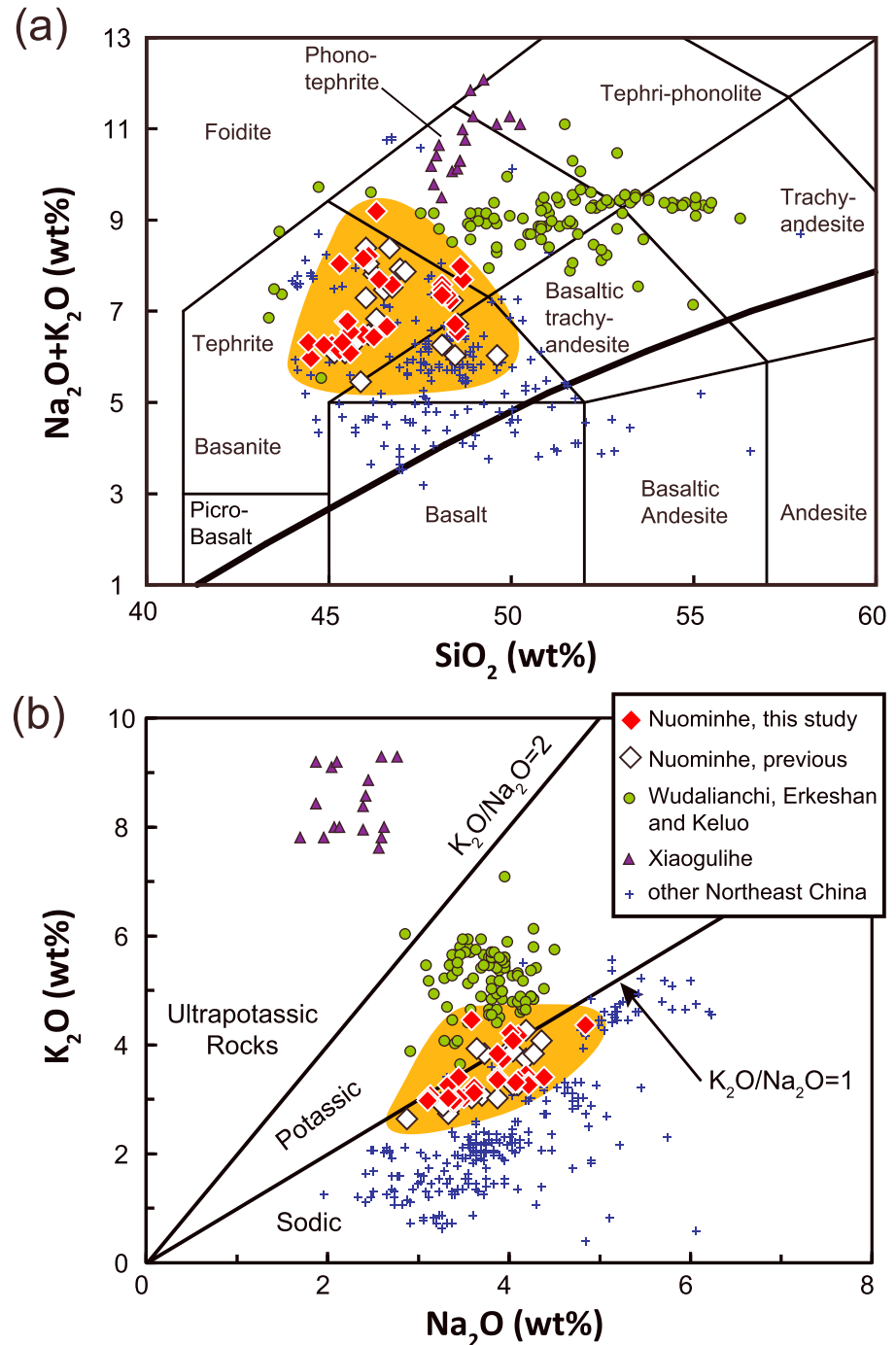
Figure 3. (a) Variation in $Na_2O + K_2O$ versus SiO_2 for the Quaternary basalt samples from the Nuominhe volcanic field. The classification of the alkaline and subalkaline series follows *Le Bas et al.* [1986]. (b) Variation of K_2O versus Na_2O for the Nuominhe basalts. The classification of ultrapotassic, potassic, and sodic rocks in K_2O/Na_2O compositional space follows *Foley et al.* [1987]. Also shown for comparison are previous data for the Nuominhe basalts [*Zhao et al.*, 2014], Wudalianchi-Erkeshan-Keluo potassic basalts [*Basu et al.*, 1991; *Fan and Hooper*, 1991; *Liu et al.*, 1994; *Zhang et al.*, 1995; *Hsu and Chen*, 1998; *Zou et al.*, 2003; *Chen et al.*, 2007; *Chu et al.*, 2013; *Kuritani et al.*, 2013], Xiaogulihe ultrapotassic rocks [*Sun et al.*, 2014], and other Cenozoic sodic volcanic rocks of Northeast China (Shuangliao, Mudanjiang, Jingpohu, Yitong, Longgang, Changbaishan, and Kuandian) [*Basu et al.*, 1991; *Fan and Hooper*, 1991; *Liu et al.*, 1994; *Hsu and Chen*, 1998; *Chen et al.*, 2007; *Yan and Zhao*, 2008; *Zou et al.*, 2008; *Kuritani et al.*, 2009; *Xu et al.*, 2012; *Chen et al.*, 2015; *Liu et al.*, 2015].
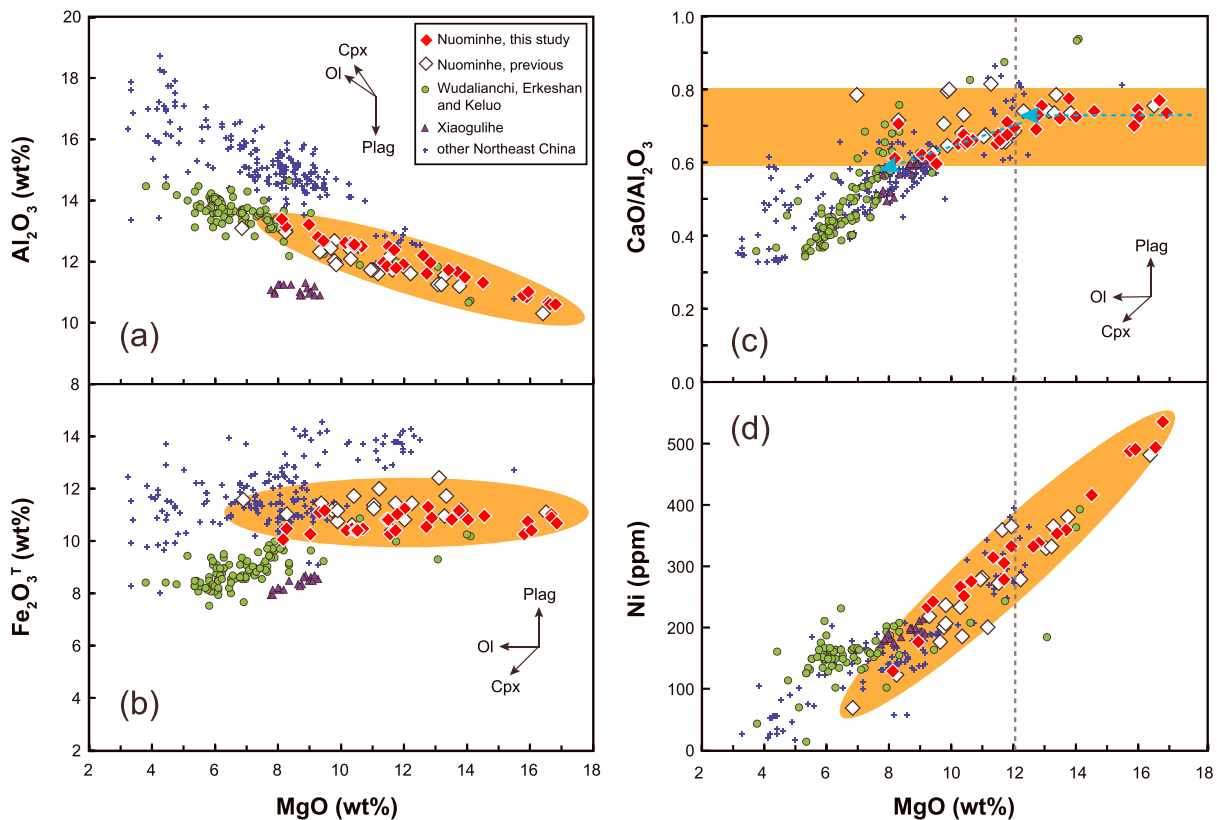
Figure 4. Variations in Al_2O_3, $Fe_2O_3^T$, CaO/Al_2O_3, and Ni versus MgO for the Nuominhe potassic basalt samples. Data for the Wudalianchi-Erkeshan-Keluo potassic basalt, the Xiaogulihe ultrapotassic rocks, and other Cenozoic sodic basalts of northeast China are from published studies as reported in Figure 3.

(Figure S1a), and they have lower Fo (75.8–88.9) and NiO contents (0.132–0.391 wt %) and higher CaO contents (0.102–0.434 wt %) and MnO contents (0.081–0.371 wt %) than the olivine xenocrysts and crystals in peridotite xenoliths entrained in the Keluo potassic basalt (Figures 7a–7c) [*Zhang et al.*, 2011]. Their CaO and MnO contents are negatively correlated with Fo (Figures 7a and 7b). Their NiO content decreases with Fo, indicating fractional crystallization, differing from a typical mantle olivine compositional array (Figure 7 c). In contrast, the olivine xenocrysts are generally anhedral (Figure S1b), and in their cores they have on average higher Fo (87.6–92.4) and NiO contents (0.320–0.435 wt %) and lower CaO contents (0.023–0.094 wt %) and MnO contents (0.032–0.170 wt %) than the phenocrysts, which are comparable to those of olivine in the Keluo mantle xenoliths (Figures 7a–7c).

Figure 7d shows the relationship between Fo content of single, microprobe analyzed olivine crystals and the whole-rock Mg# of their host basalts. The Fe^{2+}-Mg cation-partitioning coefficient between olivine and basaltic liquid varies from 0.3 at 1 atm [*Roeder and Emslie*, 1970] to 0.31–0.34 at 5–15 kbar [*Ulmer*, 1989], and the bold curves in Figure 7d indicate the range of olivine compositions that may be expected in equilibrium with a given melt composition. The upward arrow in Figure 7d indicates the effect of high-Mg xenocryst addition, while the downward arrow indicates the effect of groundmass crystallization, and the horizontal arrow indicates the effect of cognate crystal accumulation. Phenocrystic olivine core compositions for Nuominhe basalt samples 13NM11, 13NM24, 13NM29, 13NM31, and 13NM33 fall within or near the equilibrium field. However, the olivine core compositions for samples 13NM14, 13NM17, and 13NM23 fall significantly below the equilibrium field, suggesting that the analyzed olivine crystals are not equilibrium phenocrysts, but late-crystallized groundmass grains. The remaining two samples (13NM08 and 13NM25 erupted in the Middle Pleistocene and Holocene, respectively) contain two populations of olivine phenocrysts including an Mg-rich group and an equilibrium group, which plot above and within the equilibrium field. The Mg-rich olivine probably crystallized from hotter, higher-MgO melts and was entrained in the later ascending magma (i.e., they are antecrysts within the magma system).
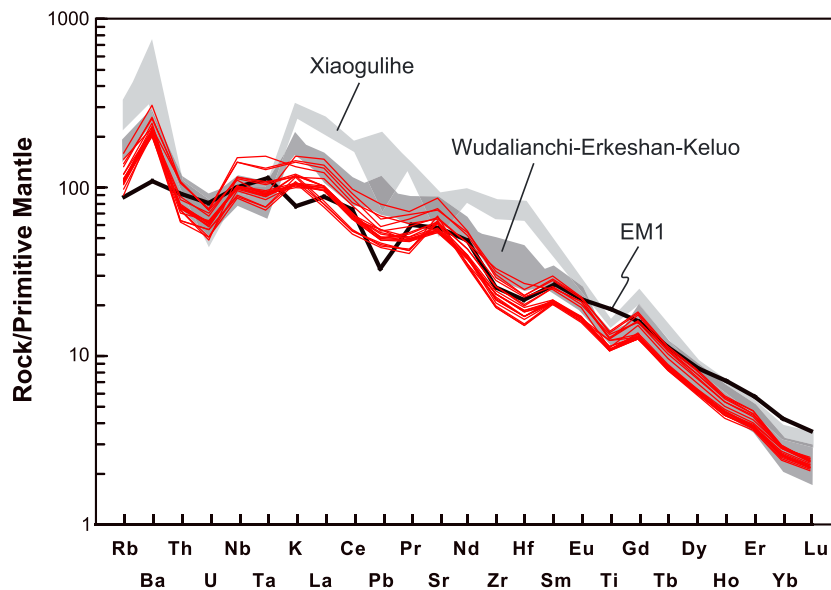
Figure 5. Primitive mantle-normalized incompatible trace element diagram for the Nuominhe basalts. The Wudalianchi-Erkeshan-Keluo potassic basalts [*Zou et al.*, 2003; *Chen et al.*, 2007; *Chu et al.*, 2013] and the Xiaogulihe ultrapotassic rocks [*Sun et al.*, 2014] are plotted for comparison. The EM1 composition (average of Tristan da Cunha) is from *Chauvel et al.* [1997]; the normalized primitive mantle composition is from *McDonough and Sun* [1995].

4. Discussion

### 4.1. Postmagmatic Alteration and Crustal Contamination

The Nuominhe high-MgO potassic basalt lavas, which erupted in the Quaternary [*Fan et al.*, 2012], appear generally fresh in hand specimen. Petrographic observation also confirms that the rocks show minor to no alteration. Only few olivine phenocrysts have been partially altered to iddingsite. In addition, good correlations between immobile incompatible elements, such as Nb, and mobile incompatible elements Rb, Th, U, Pb (Figure S4), indicate that alteration had no significant effect on whole-rock composition.

Abundant mantle xenoliths and xenocrysts are present in the Nuominhe basalt as observed in this study and in previous studies [*Sui et al.*, 2012, 2014], indicating that the magma ascended rapidly from source to surface with limited crustal assimilation. Whole-rock Nb/U and Ce/Pb compositions are high for mantle-derived melt [*Hofmann et al.*, 1986] and low for common crustal lithologies [*Rudnick and Gao*, 2003], and they are thus commonly used as markers for constraining the extent of crustal assimilation. The Nuominhe basalt samples are characterized by high Nb/U ratios (50.7–76.5) that are equivalent or higher than those of mid-ocean ridge basalt (MORB) and OIB (Figure S5a), thus ruling out significant contamination by common crustal lithologies. However, they have relatively low Ce/Pb ratios (13.0–16.5) that are intermediate between typical MORB and OIB composition, and continental crust composition (Figure S5b). If this compositional feature was the result of crustal contamination, then the Nuominhe basalts should also show a negative or positive correlation between Ce/Pb and Pb isotopes, which is not observed (Figure S5b). We therefore interpret the low Ce/Pb ratios of the Nuominhe basalts as a feature inherited from the mantle source.

4.2. The Role of Fractional Crystallization

Crystal-melt fractionation is one of the main mechanisms that may drive magma compositional evolution. For the Nuominhe high-MgO potassic basalt, the Al_2O_3 content (Figure 4a) increases sharply, the Ni (Figure 4d) and Cr (Figure S2c) contents decrease, and the $Fe_2O_3^T$ content remains nearly constant (Figure 4b) with decreasing MgO, indicating the fractionation of olivine. This is consistent with the correlated Fo-CaO-MnO-NiO composition of its olivine phenocrysts (Figure 7a–7c) and inferred chemical equilibrium between most phenocrystic olivine cores (13NM11, 13NM24, 13NM29, 13NM31, and 13NM33) and their host bulk-rock composition (Figure 7d). The low-Mg (13NM14, 13NM17, and 13NM23) and high-Mg (13NM08 and 13NM25) olivine core compositions, which are not in equilibrium with their bulk whole-rock composition (Figure 7d),
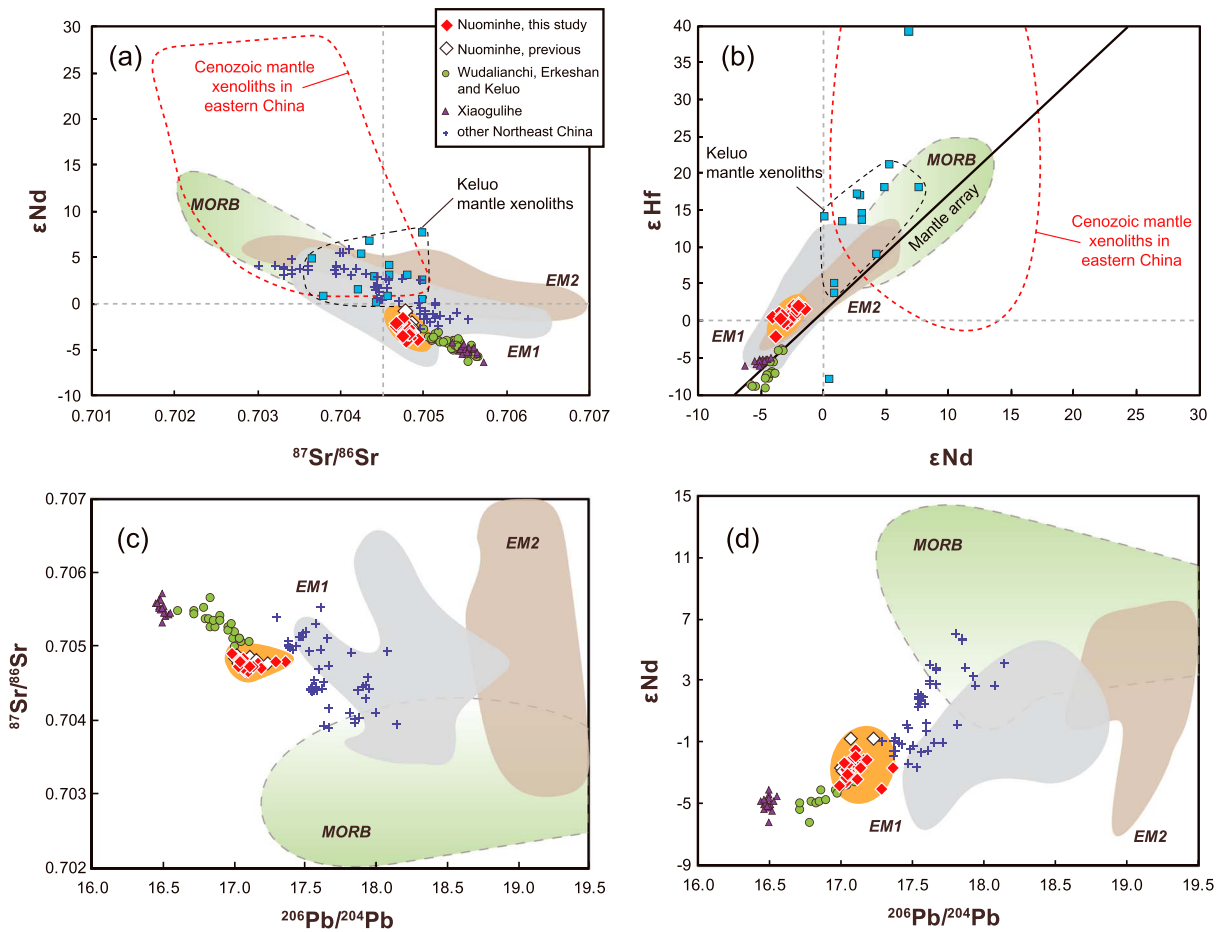
Figure 6. (a) ε_{Nd} versus $^{87}Sr/^{86}Sr$, (b) ε_{Hf} versus ε_{Nd}, (c) $^{87}Sr/^{86}Sr$ versus $^{206}Pb/^{204}Pb$, and (d) ε_{Nd} versus $^{206}Pb/^{204}Pb$ composition for the Nuominhe potassic basalts. Previous data for the Nuominhe potassic basalts [*Zhao et al.*, 2014], Wudalianchi-Erkeshan-Keluo potassic basalts [*Basu et al.*, 1991; *Zhang et al.*, 1995; *Zou et al.*, 2003; *Chu et al.*, 2013], Xiaogulihe ultrapotassic rocks [*Sun et al.*, 2014], and other Cenozoic sodic basalts from northeast China (Shuangliao, Jingpohu, Changbaishan, and Kuandian) [*Basu et al.*, 1991; *Yan and Zhao*, 2008; *Kuritani et al.*, 2009; *Xu et al.*, 2012] are plotted for comparison. Mantle xenoliths hosted by the Keluo potassic basalts [*Zhang et al.*, 2011] and other Cenozoic mantle xenoliths in eastern China [*Deng and Macdougall*, 1992; *Tatsumoto et al.*, 1992; *S. Xu et al.*, 1998; *X. Xu et al.*, 1998; *Xu et al.* 2003; *Y. Xu et al.*, 1998; *Fan et al.*, 2000; *Xu and Bodinier*, 2004; *Wu et al.*, 2006; *Zhao et al.*, 2007; *Zhou* et al., 2007, 2010; *Xiao et al.*, 2008, 2010; *Chu pet al.*, 2009; *Yu et al.*, 2009; *Liu et al.*, 2010; *Zhang et al.*, 2012; *Lu et al.*, 2013] are also plotted. Data for MORB, EM1, EM2, and HIMU composition are from GEOROC (http://georoc.mpch-mainz.gwdg.de/georoc/). The Nd-Hf isotope mantle array line in Figure 6b is from *Chauvel et al.* [2008].

represent late-crystallized groundmass and early-crystallized olivine antecrysts, respectively. The whole-rock CaO/Al$_2$O$_3$ ratios remain nearly constant at MgO > 12 wt %, while they decrease slightly at MgO < 12 wt % (Figure 4c), suggesting that clinopyroxene started to fractionate from the magma when its MgO content reached <12 wt %. However, compared to other Cenozoic potassic basalts from northeast China, the CaO/Al$_2$O$_3$ ratios of the Nuominhe basalt lavas are relatively high and narrow (0.59–0.77), indicating that the amount of clinopyroxene fractionation was limited, which is consistent with the scarcity of clinopyroxene phenocrysts in our sample suite. In addition, negative correlation between Al$_2$O$_3$ and MgO (Figure 4a), no correlation between Sr and MgO (Figure S2d), and the lack of negative Eu and Sr anomalies (Figures S3 and 5) suggest that plagioclase fractionation did not take place. We therefore conclude that most of the Nuominhe high-MgO potassic basalts have experienced olivine and minor clinopyroxene fractionation. However, for those Nuominhe basalts which contain mantle xenoliths (e.g., Banlashan and Xiaosifangshan samples), it would be difficult for the magmas to fractionate any minerals during their ascent, and they can represent the primary magma compositions. Thus, the simplex fractionational crystallization cannot explain the high and varied MgO contents (8.1–16.8 wt %) of the Nuominhe high-MgO potassic basalts, and the other processes should make a contribution (Figure 4). The basalt whole-rock compositions thus generally preserve their primitive melt characteristic [*Fan and Hooper*, 1991], and the compositions (incompatible
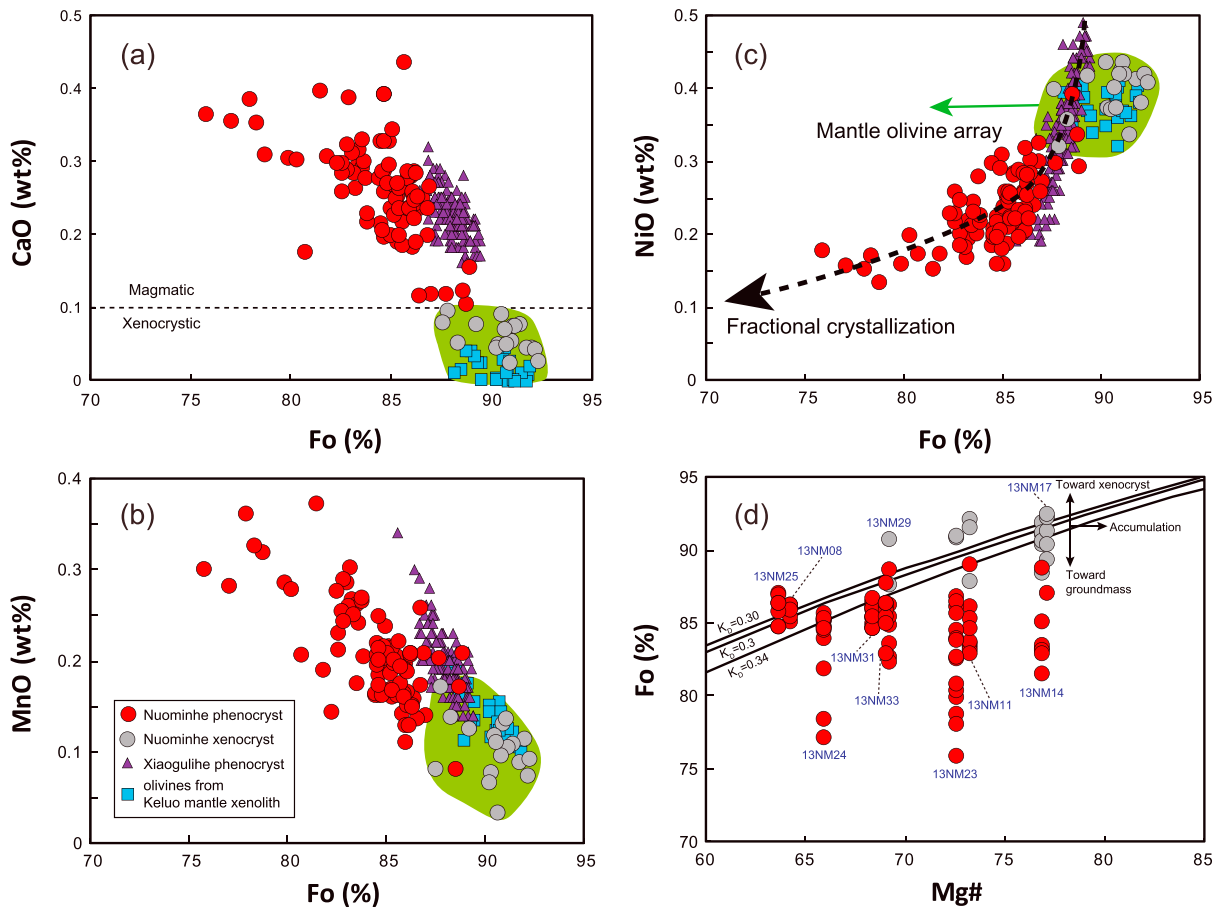
Figure 7. (a–c) Compositional variation of olivine macrocrysts from the Nuominhe potassic basalts. The dashed line separates the composition of magmatic and xenocrystic olivine on the basis of CaO [*Thompson and Gibson*, 2000]. The mantle olivine array and fractional crystallization trend in Figure 7c are from *Sato* [1977]. The olivine compositions from the Xiaogulihe ultrapotassic basalt are from *Sun et al.* [2014], and those from the Keluo xenoliths are from *Zhang et al.* [2011]. (d) Whole-rock Mg number (Mg#) versus Fo content of olivine crystals in the Nuominhe potassic basalts. Mg# = 100×Mg^{2+}/(Mg^{2+}+Fe^{2+}) calculated assuming Fe^{2+}/Fe$_{total}$ = 0.9. The Fe/Mg exchange partition coefficient between olivine and basaltic liquid varies from 0.3 at 1 atm [*Roeder and Emslie*, 1970] to 0.31–0.34 at 5–15 kbar [*Ulmer*, 1989]. Arrows indicate the relative effects of olivine xenocrysts addition (upward), accumulation (downward), and groundmass crystallization (rightward) on Fe/Mg equilibrium compositions.

trace element ratios and isotopes) are suitable to infer compositional characteristics of their mantle source and those acquired by melt-rock interaction.

4.3. Ultimate Origin of the Nuominhe Potassic Basalts

The Nuominhe high-MgO potassic basalt lavas show an elemental and isotopic composition that closely compares to that of the nearby Wudalianchi-Erkeshan-Keluo potassic and Xiaogulihe ultrapotassic rocks (Figures 4–6), indicating that all share a uniform origin. It is commonly suggested that potassic and ultrapotassic intraplate volcanic rocks represent melt directly derived from a metasomatized lithospheric mantle [*Foley et al.*, 1987; *Foley*, 1992; *Prelević et al.*, 2008, 2012]. In accordance with this interpretation and based on their high K$_2$O and lithophile element content (LREEs and large ion lithophile elements), their strongly fractionated REE content, significant ^{230}Th excess, and EM1-like isotopic characteristics, it was previously suggested that the Wudalianchi-Erkeshan-Keluo potassic and the Xiaogulihe ultrapotassic basaltic rocks were also derived from a metasomatized lithospheric mantle [*Zhang et al.*, 1995; *Zou et al.*, 2003; *Chu et al.*, 2013; *Sun et al.*, 2014; *Zhang et al.*, 2016]. Low-degree partial melting (5–7%) of phlogopite-bearing garnet peridotite at depths of 80–120 km may have generated the potassic/ultrapotassic melt [*Zhang et al.*, 1995; *Zou et al.*, 2003]. Metasomatic phlogopite has been commonly observed in mantle xenoliths from these potassic basalts [*Zhang et al.*, 2011; *Sui et al.*, 2014], which seems to support a lithospheric mantle origin for their host potassic

(and ultrapotassic) melt/lava. However, mantle xenoliths from the Keluo potassic basalts have moderately depleted Sr-Nd-Hf isotopic composition [*Zhang et al.*, 2011], and they therefore cannot be the source of these potassic and ultrapotassic lavas (Figures 6a and 6b). Furthermore, *Liu et al.* [2016] have highlighted that the Sr-Nd isotopic composition becomes less enriched, MgO content increases, and K_2O/Na_2O and Rb/Nb decrease from the Erkeshan to the Nuominhe potassic basalts with increasing lithospheric thickness below the individual volcanic fields, which also indicates that the lithospheric mantle is not the direct source of the primary potassium-enriched melts and that it modified their composition by melt-peridotite interactions. Therefore, the ultimate (primary) mantle source of the Cenozoic potassic (and ultrapotassic) basalts in northeast China, including that of the Nuominhe high-MgO potassic basalt, is located within the asthenosphere.

It further remained debated if the enriched incompatible trace element signatures and the EM1-type Sr-Nd-Pb-Hf isotopic composition of the Cenozoic potassic (and ultrapotassic) basalt in northeast China represent enriched components originated from delaminated old lower continental crust (LCC) [*Chu et al.*, 2013] or recycled ancient sediments [*Kuritani et al.*, 2013; *Sun et al.*, 2014, 2015]. The low Ce/Pb (9.4–13.5), EM1-type Sr-Nd-Hf, and low Pb isotopic composition ($^{206}Pb/^{204}Pb = 16.61$ to 17.06) have been used to support the LCC recycling model [*Chu et al.*, 2013]. However, *Sun et al.* [2014] have argued that recycled LCC cannot explain the high K_2O characteristic of the rocks, because the average K_2O content of the LCC is about 0.61 wt % only [*Rudnick and Gao*, 2003]. Partial melting of such a source thus cannot produce magma with extremely high K_2O content [*Sun et al.*, 2014]. Based on the extremely high K_2O content (>7 wt %), abnormally unradiogenic Pb isotopic composition ($^{206}Pb/^{204}Pb = 16.44–16.55$), and positive spikes of Ba, K, and Pb in the incompatible trace element patterns of the Xiaogulihe ultrapotassic rocks, it was suggested that their primary potassium-enriched melt with EM1-type geochemical signature has originated from partial melting of continental-derived sediments subducted to the mantle transition zone [*Kuritani et al.*, 2013; *Sun et al.*, 2014, 2015]. Negative mass-independent fractionation sulfur isotopic compositions (S-MIF down to $\Delta^{33}S = -0.8$) have been reported in sulfides of Pitcairn lavas, which also indicate that subducted continent-derived sediments can survive in the deep mantle for billions of years and then serve as the source components of the EM1 end-member [*Delavault et al.*, 2016]. We therefore favor the sediment recycling model rather than the LCC recycling model, while the focus of our paper is on evaluating the processes responsible for the modification of the primary melt composition, but not on identifying the origin of the mantle source.

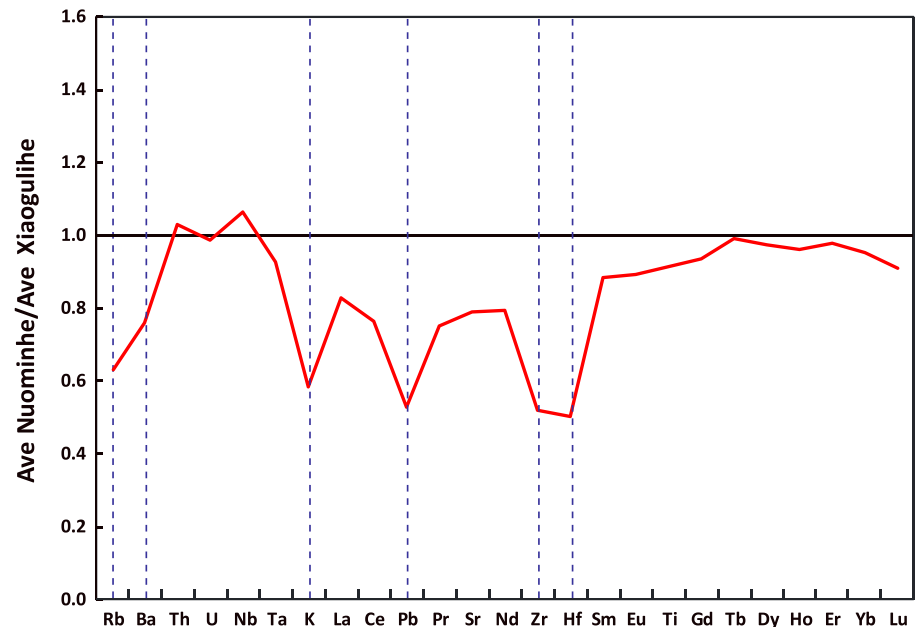### 4.4. Genesis of the Nuominhe High-MgO Potassic Basalt

That the studied Nuominhe high-MgO (8.10–16.81 wt %) potassic basaltic rocks represent melt derived from direct partial melting of recycled crustal material (i.e., continental-derived subducted sediment) is unlikely, because recycled siliciclastic sediments produce dacitic to rhyolitic partial melt compositions with high SiO_2 and low MgO contents [*Hermann and Spandler*, 2007; *Spandler et al.*, 2010; *Mallik et al.*, 2015]. However, during ascent, primary siliceous melt may interact with peridotite in the cold lithospheric mantle due to thermal and compositional disequilibrium [*Kelemen et al.*, 1990; *Yaxley and Green*, 1998; *Yaxley*, 2000; *Mallik and Dasgupta*, 2012, 2013], which would increase the MgO content and reduce the SiO_2 content of the initial melt. That magma erupted in Cenozoic volcanic field in northeast China volcanic fields has been affected by such melt-rock interaction was recently proposed by *Liu et al.* [2016] on the basis of $^{87}Sr/^{86}Sr$, MgO, K_2O/Na_2O, and Rb/Nb compositional characteristics of various potassic basalt fields and their underlying lithospheric thickness. However, mineral-scale, direct evidence for the proposed melt-rock interaction has not been investigated in detail, nor has the evolution of this process through time, as we do in the following sections.

Olivine xenocrysts captured by the Nuominhe magma show strong and relatively abrupt normal zoning with Fo- and NiO-rich and CaO- and MnO-poor core composition (Figure 2). The olivine xenocryst core composition compares to the composition of olivine in mantle xenoliths entrained by the Keluo volcanic system, while the xenocryst rims have a composition equivalent to the olivine phenocrysts with lower Fo and NiO and higher CaO and MnO contents. Olivine xenocrysts with such compositional features have also been observed by *Zhang et al.* [2016] in the Wudalianchi-Erkeshan-Keluo potassic basalt, showing plateau-like core composition with high Fo (up to 90.5) and NiO (0.35–0.38 wt %) contents and a narrow reaction/resorption rim. If entrained by hot, yet relatively evolved primary magma, the thermal and compositional disequilibrium between olivine xenocrysts and their host melt may cause olivine erosion and reaction. We interpret the
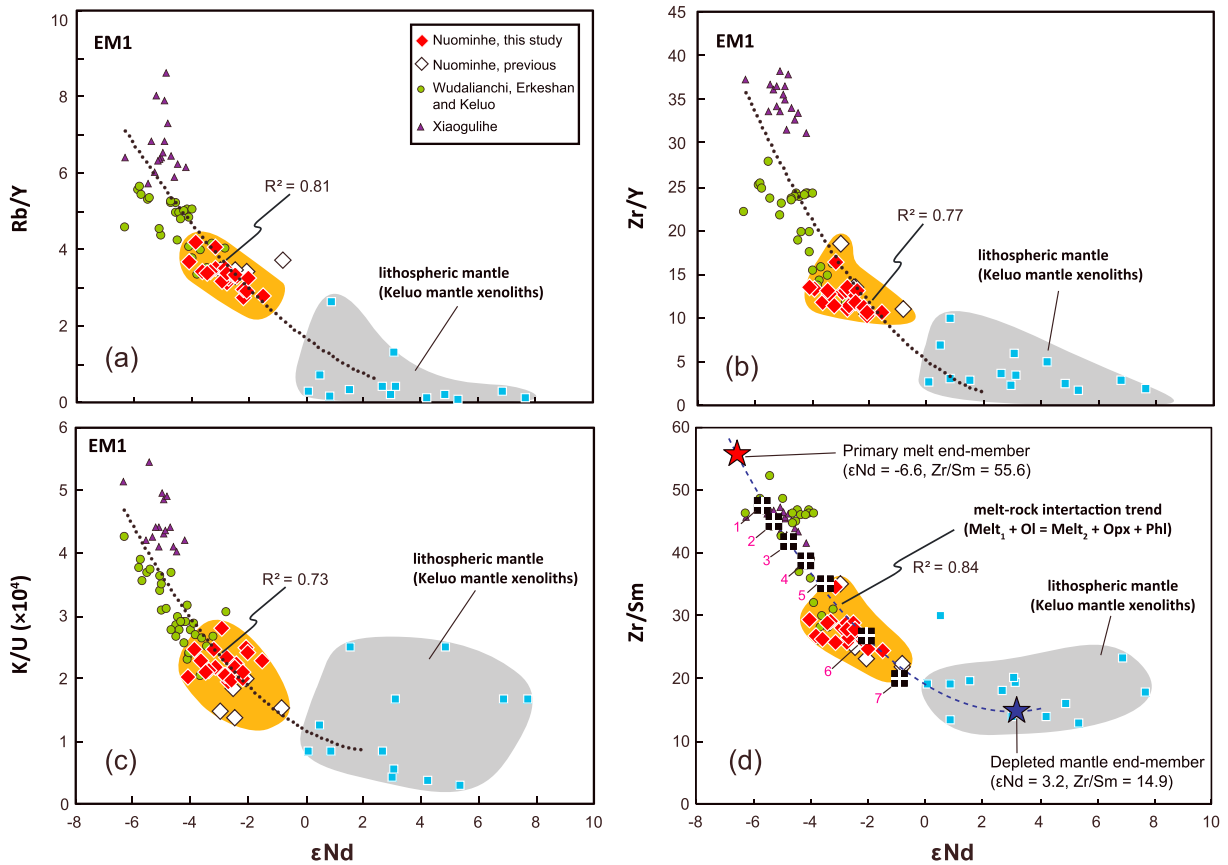
Figure 8. ε_{Nd} versus (a) Rb/Y, (b) Zr/Y, (c) K/U, and (d) Zr/Sm for the Nuominhe high-MgO potassic basalts. Also shown for comparison are previous data for the Nuominhe basalts [*Zhao et al.*, 2014], Wudalianchi-Erkeshan-Keluo potassic basalts [*Basu et al.*, 1991; *Fan and Hooper*, 1991; *Liu et al.*, 1994; *Zhang et al.*, 1995; *Hsu and Chen*, 1998; *Zou et al.*, 2003; *Chen et al.*, 2007; *Chu et al.*, 2013; *Kuritani et al.*, 2013], Xiaogulihe ultrapotassic rocks [*Sun et al.*, 2014], and Keluo mantle xenoliths [*Zhang et al.*, 2011]. The effect of melt-rock interaction (Melt$_1$ + Ol = Melt$_2$ + Opx + Phl) is quantitatively shown for ε_{Nd} and Zr/Sm compositional variation (Figure 8d). The red star (^{143}Nd/^{144}Nd = 0.5123, Nd = 50 ppm; Zr/Sm = 55.6, Zr = 556 ppm, Sm = 10 ppm) and the blue star (^{143}Nd/^{144}Nd = 0.5128, Nd = 5.5 ppm; Zr/Sm = 14.9, Zr = 5.96 ppm, Sm = 0.4 ppm) indicate the model composition of the primary melts and depleted mantle end-member, respectively. The reaction model used in this study is the assimilation-fractional crystallization formulation of *DePAOLO* [1981], where "F" is the fraction of residual melt during melt-rock interaction. The "r" value describes the relative ratio of assimilated material (olivine) to crystallized material (orthopyroxene and phlogopite). Partition coefficients for Nd, Zr, and Sm between orthopyroxene and melt are taken from *Green et al.* [2000]. Partition coefficients for Nd, Zr, and Sm between phlogopite and melt are taken from *Schmidt et al.* [1999]. Tested reaction equations were (1) 1 melt$_1$ + 0.6 Ol = 0.4 melt$_2$ + 0.3 Opx +0.7 Phl (F = 0.4, r = 0.6); (2) 1 melt$_1$ + 0.68 Ol = 0.35 melt$_2$ + 0.4 Opx +0.6 Phl (F = 0.35, r = 0.68); (3) 1 melt$_1$ + 0.75 Ol = 0.3 melt$_2$ + 0.5 Opx +0.5 Phl (F = 0.3, r = 0.75); (4) 1 melt$_1$ + 0.8 Ol = 0.25 melt$_2$ + 0.6 Opx +0.4 Phl (F = 0.25, r = 0.8); (5) 1 melt$_1$ + 0.84 Ol = 0.2 melt$_2$ + 0.8 Opx +0.2 Phl (F = 0.2, r = 0.84); (6) 1 melt$_1$ + 0.9 Ol = 0.1 melt$_2$ + 0.8 Opx +0.2 Phl (F = 0.15, r = 0.9); and (7) 1 melt$_1$ + 0.93 Ol = 0.1 melt$_2$ + 0.9 Opx +0.1 Phl (F = 0.1, r = 0.93). Model reactions with "F" varying from 0.1 to 0.4 and "r" from 0.6 to 0.93 well reproduce the compositional trends of the potassic/ultrapotassic basalts in northeast China, including the Nuominhe high-MgO potassic basalts.

irregular yet subrounded shape of the olivine xenocrysts to record such reaction [*Nakamura*, 1995; *Zhang*, 2005], and we further interpret the regular embayments in the rim zones of the olivine xenocrysts with inner subrounded outlines as evidence for partial dissolution [*Erdmann et al.*, 2014]. We propose that the reaction between olivine and melt was of the type Olivine (+ Clinopyroxene) + SiO$_2$ (melt$_1$) = Orthopyroxene (+ melt$_2$) [*Yaxley and Green*, 1998; *Mallik and Dasgupta*, 2012; *Mallik and Dasgupta*, 2013; *Mallik and Dasgupta*, 2014]. As a result of such reaction, melt MgO increases and SiO$_2$ decreases, which may account for the high-MgO and low-SiO$_2$ characteristic of the Nuominhe potassic basalt. The euhedral outer grain boundary segments of the irregular olivine rims may reflect minor partial peritectic regrowth during melt-rock interaction (in which case they could form a minor product phase in the above reaction) [*Erdmann et al.*, 2014] and/or growth during magma ascent and cooling (i.e., together with olivine phenocrysts and or matrix crystals; Figure 7d) in combination with progressive diffusive re-equilibration. Xenocryst rims with Fo contents as low as ~Fo75 compare to matrix crystal compositions thus recording late-stage crystallization and/or diffusive re-equilibration. The relatively abrupt core-rim zoning of the xenocrysts <50 μm nevertheless attest to the

Figure 9. Average incompatible trace element concentrations of the Nuominhe high-MgO potassic basalts divided by those of the Erkeshan potassic basalts. This shows that Rb, Ba, K, Pb, Zr, and Hf are depleted as a result of the reactive crystallization of phlogopite through the interaction of asthenospheric potassic melts with the subcontinental lithospheric mantle.

rapid ascent of the magmas as diffusion in olivine is fast [*Chakraborty*, 1997; *Petry* et al., 2004; *Coogan et al.*, 2005; *Dohmen and Chakraborty*, 2007; *Dohmen et al.*, 2007].

Intergranular phlogopite that commonly occurs as a metasomatic phase in garnet peridotite xenoliths entrained in the Nuominhe basalt has high K_2O (8.42–10.14 wt %) and TiO_2 (5.41–7.79 wt %) content [*Sui et al.*, 2014], which is interpreted to record the interaction between potassic melt and peridotite in the cold lithospheric mantle beneath the Nuominhe volcanic field [*Liu et al.*, 2016]. Such phlogopite also commonly occurs in mantle xenoliths entrained by the Keluo potassic basalts [*Zhang et al.*, 2011], suggesting K metasomatism is common in the lithospheric mantle beneath these potassic volcanic fields. Low $(La/Yb)_N$ (0.45–6.17) but high Ti/Eu (765–6051) composition of clinopyroxene in the Keluo mantle xenoliths is consistent with metasomatic crystallization in reaction with silicate melts rather than carbonatite melts [*Zhang et al.*, 2011]. Moreover, these mantle xenoliths have less depleted Sr-Nd isotopic compositions than mantle xenoliths from Cenozoic sodic basalts in eastern China (Figure 6a [*Zhang et al.*, 2011]), which indicates that the metasomatic melts have enriched their Sr-Nd isotopic composition. The K metasomatism can thus be explained by reaction between depleted lithospheric mantle and potassic silicate melt represented by the host potassic lavas. Potassic metasomatism can enrich Rb in the lithospheric mantle, yet these phlogopite-bearing mantle xenoliths have more depleted Sr isotopes ($^{87}Sr/^{86}Sr < 0.7049$) relative to their host potassic lavas (Figure 6a), which is consistent with a recent, and as we infer, a metasomatic event concurrent with ascent and volcanic activity at the Nuominhe volcanic field.

In addition, the Cenozoic potassic (and ultrapotassic) basalts and Keluo mantle xenoliths from the northeast China define an array in ε_{Nd} and trace element ratios (Rb/Y, Zr/Y, Zr/Sm, and K/U) from enriched potassic melts to a depleted lithospheric mantle composition (Figure 8). The Nuominhe high-MgO potassic basalts lie in the central part of the array with moderate ε_{Nd} and Rb/Y, Zr/Y, Zr/Sm, and K/U ratios, further supporting the interpretation of their genesis by melt-rock reaction between enriched potassic melt and cold, subcontinental lithospheric mantle (SCLM). The primitive, yet enriched potassic melts with high Rb/Y, Zr/Y, K/U, and Zr/Sm ratios are characteristic for the EM1 end-member in Northeast China, which were probably derived from recycled ancient sediments [*Kuritani et al.*, 2011, 2013; *Sun et al.*, 2014, 2015]. To quantify the contribution of the depleted SCLM to the primary enriched potassic melts in the formation of Nuominhe basalts, we use their ε_{Nd} and Zr/Sm composition and the reaction model ($Melt_1 + Olivine = Melt_2 + Orthopyroxene$
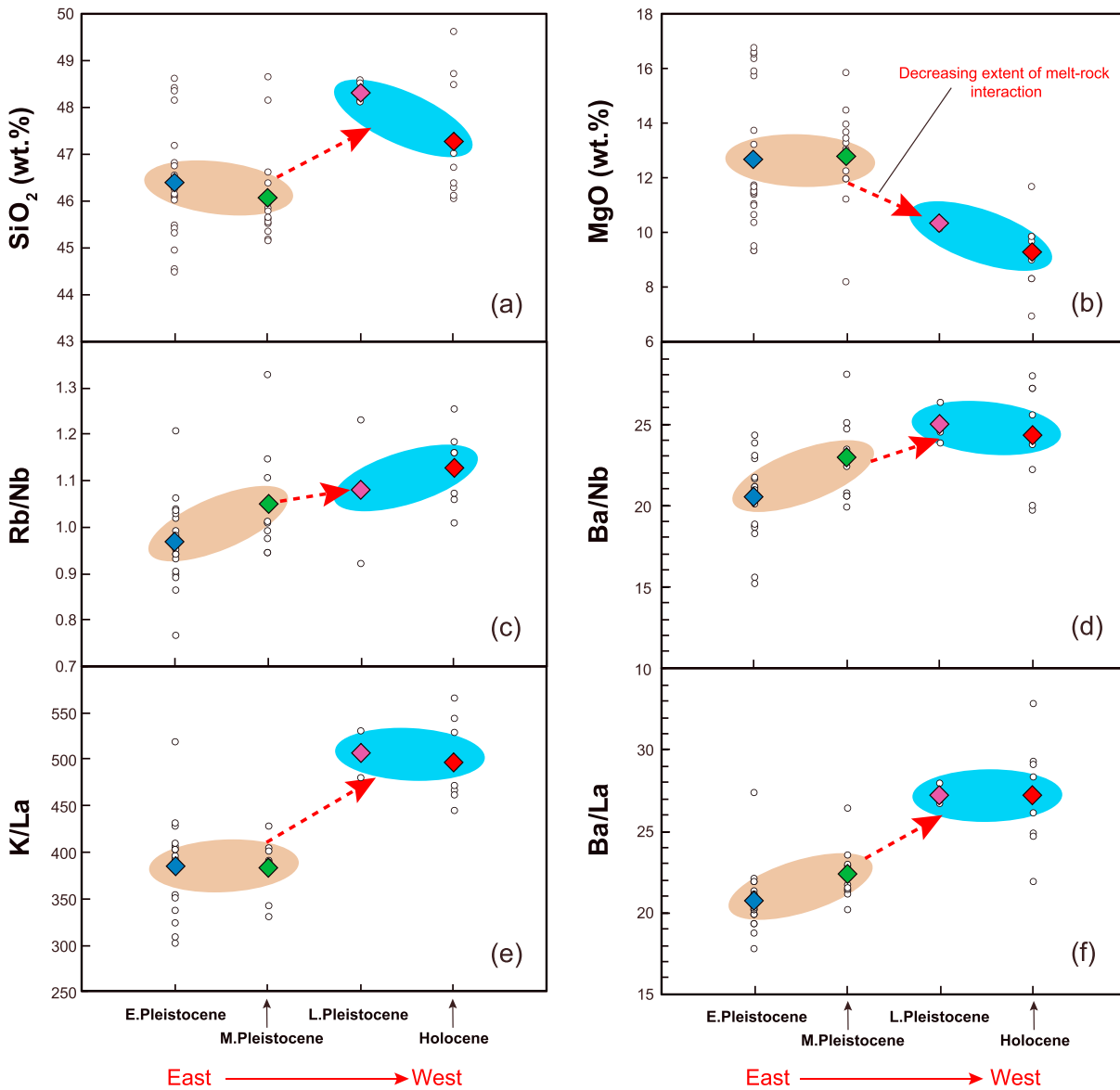
Figure 10. Variation of (a) SiO$_2$, (b) MgO, (c) Rb/Nb, (d) Ba/Nb, (e) K/La, and (f) Ba/La of the Nuominhe high-MgO potassic basaltic rocks with their eruptive episodes. Small white circles represent all samples which include those of *Zhao et al.* [2014] and this study. Colored diamonds represent mean values of each group.

+ Phlogopite) following the assimilation-fractional crystallization formulation of *DePaolo* [1981] (Figure 8d). The results show that melt-rock interaction between primary enriched melts (^{143}Nd/^{144}Nd = 0.5123, Nd = 50 ppm; Zr/Sm = 55.6) and a depleted mantle component (^{143}Nd/^{144}Nd = 0.5128, Nd = 5.5 ppm; Zr/Sm = 14.9) well reproduce the geochemical variations of the Nuominhe lavas at the fraction of residual melt of ~0.1–0.2 and at the relative ratio of assimilated material (olivine) to crystallized material (orthopyroxene and phlogopite) of ~0.84–0.93 (Figure 8d). Comparisons between average trace element concentrations from the Nuominhe basalts and those from the Erkeshan potassic basalts [*Chu et al.*, 2013] further show that Rb, Ba, K, Pb, Zr, and Hf became depleted through the interaction of the asthenospheric potassic melts with the SCLM (Figure 9).

4.5. Temporal Evolution of the Nuominhe High-MgO Potassic Basalt

On the basis of their chemical variation with eruptive age (Figure 10), the Nuominhe basalt lavas can be subdivided into two stages: an early eruption stage including Early Pleistocene and Middle Pleistocene lavas and a late eruption stage including Late Pleistocene and Holocene lavas. The average SiO$_2$, Rb/Nb, Ba/Nb, K/La,
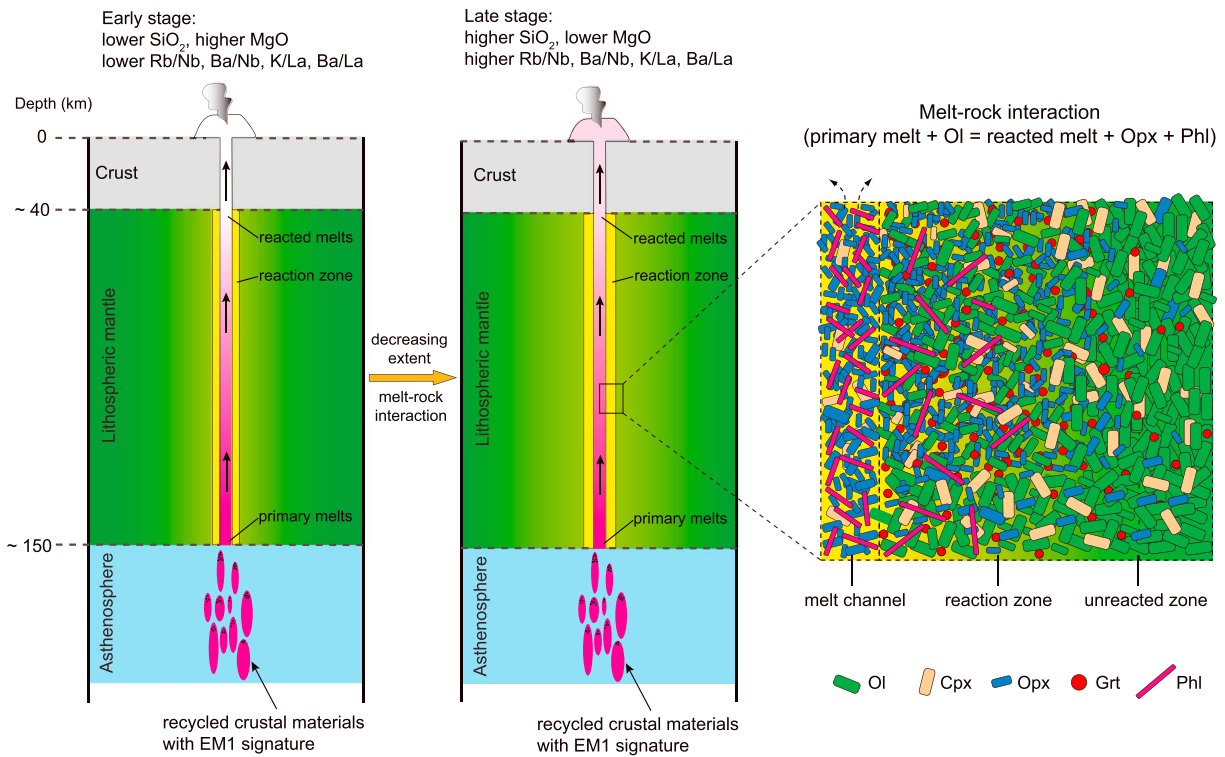
Figure 11. Schematic illustrations showing the components and formation process proposed for the Nuominhe high-MgO potassic basalts from the Greater Khingan Range. We suggest that primary silica- and potassium-rich melts were generated in the upmost asthenosphere from recycled crustal material with EM1 signature. When this melt ascended through the lithospheric mantle, melt-rock interaction occurred that partially consumed olivine of the host rocks and precipitated orthopyroxene and phlogopite. As a result, the MgO content of the ascending melt increased and SiO_2, Rb/Nb, Ba/Nb, K/La, and Ba/La decreased. With time, the reaction zone between melt channel and unreacted host rocks sealed the host rock-melt system from further reaction and the composition of the ascending melt changed less during the late stage than during the early stage. Thus, the extent of melt-rock interaction decreased with time, resulting in an increase in whole-rock SiO_2, Rb/Nb, Ba/Nb, K/La, and Ba/La and a decrease in whole-rock MgO contents from early erupted lavas (Early Pleistocene and Middle Pleistocene) to late erupted lavas (Late Pleistocene and Holocene).

and Ba/La contents increase, while the MgO content decreases from the early stage to the late stage lavas (Figure 10). As recorded by mantle xenoliths in potassic basalts of the NVF, phlogopite appears to have precipitated when the potassic melt ascended through the lithospheric mantle [*Sui et al.*, 2014]. Because Rb, Ba, and K are compatible in phlogopite while Nb and La are incompatible, the precipitation of phlogopite in the lithospheric mantle decreases Rb/Nb, Ba/Nb, Ba/La and K/La ratios of the resulting melt. The compositional variation of the reacted melt depends on the extent of melt-rock interaction and the reactant assemblage. If magma pathways through the lithosphere remain active for prolonged periods, reaction zones between melt channels and unreacted peridotite will be established, first slowing and eventually preventing further reaction. Magma that erupted in the early stage during which the NVF magma plumbing system was established will have had significant opportunity to react with the lithospheric mantle upon its ascent. Magma erupted in the following and up to the Holocene may have had comparatively minor reactive interaction with the depleted lithospheric mantle, thus, limiting the amount of phlogopite formation and reactive depletion of the ascending melt in Rb, Ba, and K, resulting in an increase of Rb/Nb, Ba/Nb, K/La, and Ba/La from the oldest to the youngest erupted magma of the volcanic field.

Figure 11 summarizes our interpretation of the formation of the Nuominhe potassic basalt magma from source to surface. We suggest that primary silica- and potassium-rich melt with EM1 elemental and isotopic character was generated in the upmost asthenosphere. Melt-peridotite interaction occurred when this melt ascended through the lithospheric mantle, owing to thermal and compositional disequilibrium. This reaction consumed olivine and precipitated orthopyroxene and phlogopite, leading to an increase of melt MgO and a decrease of melt SiO_2 and Rb/Nb, Ba/Nb, K/La, and Ba/La. With time, the reaction between ascending melt and peridotite will have effectively isolated peridotite from the ascending melt, eventually forming a reaction

zone and preventing further reaction. Magma erupted during the late stage (late Pleistocene and Holocene) were therefore less significantly modified by melt-rock interaction, and they are thus characterized by higher SiO_2, Rb/Nb, Ba/Nb, K/La, Ba/La, and lower MgO contents than that magmas erupted during the early stage (early and middle Pleistocene) (Figure 11).

5. Conclusions

Quaternary high-MgO potassic basalts erupted in the Nuominhe volcanic field from the Greater Khingan Range are predominantly basanite with low SiO_2 content ($SiO_2 = 44.4$–48.7 wt %) and high alkali content ($K_2O + Na_2O = 6.0$–9.2 wt %). They have the highest MgO content (8.2–16.8 wt %) among Cenozoic basalt in northeastern China. These basalts are characterized by EM1-like incompatible trace element patterns and Sr-Nd-Pb-Hf isotopic compositions. Whole-rock composition in combination with mineral assemblages of mantle-derived xenoliths and partially resorbed olivine xenocrysts in the basaltic rocks provides evidence that melt-rock reaction played an important role in the formation of the Nuominhe potassic basalt. Increasing SiO_2, Rb/Nb, Ba/Nb, Ba/La, and K/La and decreasing MgO contents of lava erupted in the early stage (Early Pleistocene and Middle Pleistocene) to lava that erupted in the late stage (Late Pleistocene and Holocene) reflect progressively decreasing melt-rock interaction in the lithospheric mantle with longevity of the volcanic magma system.

References

Basu, A. R., J. Wang, W. Huang, G. Xie, and M. Tatsumoto (1991), Major element, REE, and Pb, Nd and Sr isotopic geochemistry of Cenozoic volcanic rocks of eastern China: Implications for their origin from suboceanic-type mantle reservoirs, *Earth Planet. Sci. Lett.*, *105*, 149–169.

Chakraborty, S. (1997), Rates and mechanisms of Fe-Mg interdiffusion in olivine at 980°–1300°C, *J. Geophys. Res.*, *102*, 12,317–12,331, doi:10.1029/97JB00208.

Chauvel, C., W. McDonough, G. Guille, R. Maury, and R. Duncan (1997), Contrasting old and young volcanism in Rurutu Island, Austral chain, *Chem. Geol.*, *139*, 125–143.

Chauvel, C., E. Lewin, M. Carpentier, N. T. Arndt, and J. Marini (2008), Role of recycled oceanic basalt and sediment in generating the Hf–Nd mantle array, *Nat. Geosci.*, *1*, 64–67.

Chen, S., Q. Fan, H. Zou, Y. Zhao, and R. Shi (2015), Geochemical and Sr–Nd isotopic constraints on the petrogenesis of late Cenozoic basalts from the Abaga area, Inner Mongolia, eastern China, *J. Volcanol. Geotherm. Res.*, *305*, 30–44.

Chen, Y., Y. Zhang, D. Graham, S. Su, and J. Deng (2007), Geochemistry of Cenozoic basalts and mantle xenoliths in Northeast China, *Lithos*, *96*, 108–126.

Choi, S. H., S. B. Mukasa, S. Kwon, and A. V. Andronikov (2006), Sr, Nd, Pb and Hf isotopic compositions of late Cenozoic alkali basalts in South Korea: Evidence for mixing between the two dominant asthenospheric mantle domains beneath East Asia, *Chem. Geol.*, *232*, 134–151.

Chu, Z., F. Wu, R. J. Walker, R. L. Rudnick, L. Pitcher, I. S. Puchtel, Y. Yang, and S. A. Wilde (2009), Temporal evolution of the lithospheric mantle beneath the eastern North China Craton, *J. Petrol.*, *50*, 1857–1898.

Chu, Z., J. Harvey, C. Liu, J. Guo, F. Wu, W. Tian, Y. Zhang, and Y. Yang (2013), Source of highly potassic basalts in northeast China: Evidence from Re–Os, Sr–Nd–Hf isotopes and PGE geochemistry, *Chem. Geol.*, *357*, 52–66.

Coogan, L. A., A. Hain, S. Stahl, and S. Chakraborty (2005), Experimental determination of the diffusion coefficient for calcium in olivine between 900°C and 1500°C, *Geochim. Cosmochim. Acta*, *69*(14), 3683–3694.

Delavault, H., C. Chauvel, E. Thomassot, C. W. Devey, and B. Dazas (2016), Sulfur and lead isotopic evidence of relic Archean sediments in the Pitcairn mantle plume, *Proc. Natl. Acad. Sci. U.S.A.*, *113*, 12,952–12,956.

Deng, F., and J. D. Macdougall (1992), Proterozoic depletion of the lithosphere recorded in mantle xenoliths from Inner Mongolia, *Nature*, *360*, 333–336.

DePaolo, D. J. (1981), Trace element and isotopic effects of combined wallrock assimilation and fractional crystallization, *Earth Planet. Sci. Lett.*, *53*(2), 189–202.

Dohmen, R., and S. Chakraborty (2007), Fe–Mg diffusion in olivine II: Point defect chemistry, change of diffusion mechanisms and a model for calculation of diffusion coefficients in natural olivine, *Phys. Chem. Miner.*, *34*(6), 409–430.

Dohmen, R., H. Becker, and S. Chakraborty (2007), Fe–Mg diffusion in olivine I: experimental determination between 700 and 1,200°C as a function of composition, crystal orientation and oxygen fugacity, *Phys. Chem. Miner.*, *34*(6), 389–407.

Erdmann, S., B. Scaillet, C. Martel, and A. Cadoux (2014), Characteristic textures of recrystallized, peritectic, and primary magmatic olivine in experimental samples and natural volcanic rocks, *J. Petrol.*, *55*(12), 2377–2402.

Fan, Q., and P. R. Hooper (1991), The Cenozoic basaltic rocks of eastern China: Petrology and chemical composition, *J. Petrol.*, *32*, 765–810.

Fan, Q., Y. W. Zhao, J. L. Sui, D. M. Li, and Y. Wu (2012), Studies on Quaternary volcanism stages of Nuomin river area in the Great Xing'an Range: Evidence from petrology, K-Ar dating and volcanic geology features, *Acta Petrol. Sin.*, *28*, 1092–1098.

Fan, W. M., H. F. Zhang, J. Baker, K. E. Jarvis, P. Mason, and M. A. Menzies (2000), On and off the North China Craton: Where is the Archaean keel?, *J. Petrol.*, *41*, 933–950.

Foley, S. (1992), Petrological characterization of the source components of potassic magmas: Geochemical and experimental constraints, *Lithos*, *28*, 187–204.

Foley, S. F., G. Venturelli, D. H. Green, and L. Toscani (1987), The ultrapotassic rocks: characteristics, classification, and constraints for petrogenetic models, *Earth Sci. Rev.*, *24*, 81–134.

Green, T. H., J. D. Blundy, J. Adam, and G. M. Yaxley (2000), SIMS determination of trace element partition coefficients between garnet, clinopyroxene and hydrous basaltic liquids at 2–7.5 GPa and 1080–1200°C, *Lithos*, *53*(3), 165–187.

Guo, Z., Y. Cao, X. Wang, Y. John Chen, J. Ning, W. He, Y. Tang, and Y. Feng (2014), Crust and upper mantle structures beneath Northeast China from receiver function studies, *Earthquake Sci.*, *27*, 265–275.

Hermann, J., and C. J. Spandler (2007), Sediment melts at sub-arc depths: An experimental study, *J. Petrol.*, *49*(4), 717–740.

Ho, K., W. Ge, J. Chen, C. You, H. Yang, and Y. Zhang (2013), Late Cenozoic magmatic transitions in the central Great Xing'an Range, Northeast China: Geochemical and isotopic constraints on petrogenesis, *Chem. Geol.*, *352*, 1–18.

Hofmann, A. W. (1997), Mantle geochemistry: The message from oceanic volcanism, *Nature*, *385*, 219–229.

Hofmann, A. W. (2003), Sampling mantle heterogeneity through oceanic basalts: Isotopes and trace elements, *Treatise Geochem.*, *2*, 568.

Hofmann, A. W., and W. M. White (1982), Mantle plumes from ancient oceanic crust, *Earth Planet. Sci. Lett.*, *57*, 421–436.

Hofmann, A. W., K. P. Jochum, M. Seufert, and W. M. White (1986), Nb and Pb in oceanic basalts: New constraints on mantle evolution, *Earth Planet. Sci. Lett.*, *79*, 33–45.

Hsu, C., and J. Chen (1998), Geochemistry of late Cenozoic basalts from Wudalianchi and Jingpohu areas, Heilongjiang Province, northeast China, *J. Asian Earth Sci.*, *16*, 385–405.

Jahn, B., F. Wu, and B. Chen (2000), Granitoids of the Central Asian Orogenic Belt and continental growth in the Phanerozoic, *Geol. Soc. Am. Spec. Pap.*, *350*, 181–193.

Kelemen, P. B., D. B. Joyce, J. D. Webster, and J. R. Holloway (1990), Reaction between ultramafic rock and fractionating basaltic magma II. Experimental investigation of reaction between olivine tholeiite and harzburgite at 1150–1050°C and 5kb, *J. Petrol.*, *31*, 99–134.

Kuritani, T., and E. Nakamura (2002), Precise isotope analysis of nanogram-level Pb fornatural rock samples without use of double spikes, *Chem. Geol.*, *186*, 31–43.

Kuritani, T., J. Kimura, T. Miyamoto, H. Wei, T. Shimano, F. Maeno, X. Jin, and H. Taniguchi (2009), Intraplate magmatism related to deceleration of upwelling asthenospheric mantle: Implications from the Changbaishan shield basalts, northeast China, *Lithos*, *112*, 247–258.

Kuritani, T., E. Ohtani, and J. Kimura (2011), Intensive hydration of the mantle transition zone beneath China caused by ancient slab stagnation, *Nat. Geosci.*, *4*, 713–716.

Kuritani, T., J. Kimura, E. Ohtani, H. Miyamoto, and K. Furuyama (2013), Transition zone origin of potassic basalts from Wudalianchi volcano, northeast China, *Lithos*, *156–159*, 1–12.

Lambart, S., D. Laporte, A. Provost, and P. Schiano (2012), Fate of pyroxenite-derived melts in the peridotitic mantle: Thermodynamic and experimental constraints, *J. Petrol.*, *53*, 451–476.

Le Bas, M. J., R. W. Le Maitre, A. Streckeisen, and B. Zanettin (1986), A chemical classification of volcanic rocks based on the total alkali-silica diagram, *J. Petrol.*, *27*, 745–750.

Liu, C., A. Masuda, and G. Xie (1994), Major- and trace-element compositions of Cenozoic basalts in eastern China: Petrogenesis and mantle source, *Chem. Geol.*, *114*, 19–42.

Liu, J., J. Han, and W. S. Fyfe (2001), Cenozoic episodic volcanism and continental rifting in northeast China and possible link to Japan Sea development as revealed from K–Ar geochronology, *Tectonophysics*, *339*, 385–401.

Liu, J., L. Chen, G. Zeng, X. Wang, Y. Zhong, and X. Yu (2016), Lithospheric thickness controlled compositional variations in potassic basalts of Northeast China by melt-rock interactions, *Geophys. Res. Lett.*, *43*, 2582–2589, doi:10.1002/2016GL068332.

Liu, J., S. Chen, Z. Guo, W. Guo, H. He, H. You, H. Kim, G. Sung, and H. Kim (2015), Geological background and geodynamic mechanism of Mt. Changbai volcanoes on the China–Korea border, *Lithos*, *236–237*, 46–73.

Liu, Z., F. Y. Wu, Z. Y. Chu, and X. S. Xu (2010), Isotopic compositions of the peridotite xenoliths from the Nushan area, Anhui Province: Constraints on the age of subcontinental lithospheric mantle beneath the East China, *Acta Petrol. Sin.*, *26*, 1217–1240.

Lu, J., J. Zheng, W. L. Griffin, and C. Yu (2013), Petrology and geochemistry of peridotite xenoliths from the Lianshan region: Nature and evolution of lithospheric mantle beneath the lower Yangtze block, *Gondwana Res.*, *23*, 161–175.

Ma, X. (1987), *Lithospheric Dynamics Map of China and Adjacent Seas: 1: 4 000 000 and Explanatory Notes*, pp. 53, Geol. House, Beijing.

Mallik, A., and R. Dasgupta (2012), Reaction between MORB-eclogite derived melts and fertile peridotite and generation of ocean island basalts, *Earth Planet. Sci. Lett.*, *329–330*, 97–108.

Mallik, A., and R. Dasgupta (2013), Reactive infiltration of MORB-eclogite-derived carbonated silicate melt into fertile peridotite at 3 GPa and genesis of alkalic magmas, *J. Petrol.*, *54*, 2267–2300.

Mallik, A., and R. Dasgupta (2014), Effect of variable CO$_2$ on eclogite-derived andesite and lherzolite reaction at 3 GPa-Implications for mantle source characteristics of alkalic ocean island basalts, *Geochem. Geophys. Geosyst.*, *15*, 1533–1557, doi:10.1002/2014GC005251.

Mallik, A., J. Nelson, and R. Dasgupta (2015), Partial melting of fertile peridotite fluxed by hydrous rhyolitic melt at 2–3 GPa: Implications for mantle wedge hybridization by sediment melt and generation of ultrapotassic magmas in convergent margins, *Contrib. Mineral. Petrol.*, *169*, 48.

McDonough, W. F., and S. Sun (1995), The composition of the Earth, *Chem. Geol.*, *120*, 223–253.

McKenzie, D., and R. K. O'Nions (1991), Partial melt distributions from inversion of rare earth element concentrations, *J. Petrol.*, *32*, 1021–1091.

Nakamura, M. (1995), Residence time and crystallization history of nickeliferous olivine phenocrysts from the northern Yatsugatake volcanoes, Central Japan: Application of a growth and diffusion model in the system Mg-Fe-Ni, *J. Volcanol. Geotherm. Res.*, *66*, 81–100.

Petry, C., S. Chakraborty, and H. Palme (2004), Experimental determination of Ni diffusion coefficients in olivine and their dependence on temperature, composition, oxygen fugacity, and crystallographic orientation, *Geochim. Cosmochim. Acta*, *68*(20), 4179–4188.

Prelević, D., S. F. Foley, R. Romer, and S. Conticelli (2008), Mediterranean Tertiary lamproites derived from multiple source components in postcollisional geodynamics, *Geochim. Cosmochim. Acta*, *72*, 2125–2156.

Prelević, D., C. Akal, S. F. Foley, R. L. Romer, A. Stracke, and P. Van Den Bogaard (2012), Ultrapotassic mafic rocks as geochemical proxies for post-collisional dynamics of orogenic lithospheric mantle: The case of southwestern Anatolia, Turkey, *J. Petrol.*, *53*, 1019–1055.

Roeder, P. L., and R. Emslie (1970), Olivine-liquid equilibrium, *Contrib. Mineral. Petrol.*, *29*, 275–289.

Rudnick, R. L., and S. Gao (2003), Composition of the continental crust, *Treatise Geochem.*, *3*, 1–64.

Sato, H. (1977), Nickel content of basaltic magmas: Identification of primary magmas and a measure of the degree of olivine fractionation, *Lithos*, *10*, 113–120.

Schmidt, K. H., P. Bottazzi, R. Vannucci, and K. Mengel (1999), Trace element partitioning between phlogopite, clinopyroxene and leucite lamproite melt, *Earth Planet. Sci. Lett.*, *168*(3), 287–299.

Sengor, A., and B. A. Natalin (1996), *Paleotectonics of Asia: Fragments of a Synthesis*, Cambridge Univ. Press, Cambridge.

Sengör, A., B. A. Natal'In, and V. S. Burtman (1993), Evolution of the Altaid tectonic collage and Palaeozoic crustal growth in Eurasia, *Nature*, *364*, 299–307.

Søager, N., and P. M. Holm (2013), Melt–peridotite reactions in upwelling eclogite bodies: Constraints from EM1-type alkaline basalts in Payenia, Argentina, *Chem. Geol.*, *360–361*, 204–219.

Søager, N., P. M. Holm, and E. J. Llambías (2013), Payenia volcanic province, southern Mendoza, Argentina: OIB mantle upwelling in a backarc environment, *Chem. Geol.*, *349–350*, 36–53.

Sobolev, A. V., A. W. Hofmann, S. V. Sobolev, and I. K. Nikogosian (2005), An olivine-free mantle source of Hawaiian shield basalts, *Nature*, *434*, 590–597.

Sobolev, A. V., A. W. Hofmann, D. V. Kuzmin, G. M. Yaxley, N. T. Arndt, S. Chung, L. V. Danyushevsky, T. Elliott, F. A. Frey, and M. O. Garcia (2007), The amount of recycled crust in sources of mantle-derived melts, *Science*, *316*, 412–417.

Spandler, C., G. Yaxley, D. H. Green, and D. Scott (2010), Experimental phase and melting relations of metapelite in the upper mantle: Implications for the petrogenesis of intraplate magmas, *Contrib. Mineral. Petrol.*, *160*(4), 569–589.

Stracke, A. (2012), Earth's heterogeneous mantle: A product of convection-driven interaction between crust and mantle, *Chem. Geol.*, *330–331*, 274–299.

Sui, J. L., Q. C. Fan, and Y. G. Xu (2012), Discovery of peridotite xenoliths from the Nuomin river Quaternary volcanic field, the Great Xing'an Range, and its geological significance, *Acta Petrol. Sin.*, *28*, 1130–1138.

Sui, J. L., N. Li, Q. C. Fan, and Y. G. Xu (2014), Phlogopites and potassic melts in mantle xenoliths from Nuomin volcanic field, northern Great Xing'an Range, *Acta Petrol. Sin.*, *30*, 3587–3594.

Sun, Y., J. Ying, B. Su, X. Zhou, and J. Shao (2015), Contribution of crustal materials to the mantle sources of Xiaogulihe ultrapotassic volcanic rocks, Northeast China: New constraints from mineral chemistry and oxygen isotopes of olivine, *Chem. Geol.*, *405*, 10–18.

Sun, Y., J. Ying, X. Zhou, J. Shao, Z. Chu, and B. Su (2014), Geochemistry of ultrapotassic volcanic rocks in Xiaogulihe NE China: Implications for the role of ancient subducted sediments, *Lithos*, *208–209*, 53–66.

Tang, J., W. Xu, F. Wang, W. Wang, M. Xu, and Y. Zhang (2014), Geochronology and geochemistry of Early–Middle Triassic magmatism in the Erguna Massif, NE China: Constraints on the tectonic evolution of the Mongol–Okhotsk Ocean, *Lithos*, *184*, 1–16.

Tang, Y., H. Zhang, and J. Ying (2006), Asthenosphere–lithospheric mantle interaction in an extensional regime: Implication from the geochemistry of Cenozoic basalts from Taihang Mountains, North China Craton, *Chem. Geol.*, *233*, 309–327.

Tao, K., F. Niu, J. Ning, Y. J. Chen, S. Grand, H. Kawakatsu, S. Tanaka, M. Obayashi, and J. Ni (2014), Crustal structure beneath NE China imaged by NECESSArray receiver function data, *Earth Planet. Sci. Lett.*, *398*, 48–57.

Tatsumoto, M., A. R. Basu, H. Wankang, W. Junwen, and X. Guanghong (1992), Sr, Nd, and Pb isotopes of ultramafic xenoliths in volcanic rocks of Eastern China: Enriched components EMI and EMII in subcontinental lithosphere, *Earth Planet. Sci. Lett.*, *113*, 107–128.

Thompson, R. N., and S. A. Gibson (2000), Transient high temperatures in mantle plume heads inferred from magnesian olivines in Phanerozoic picrites, *Nature*, *407*, 502–506.

Ulmer, P. (1989), The dependence of the Fe2 + −Mg cation-partitioning between olivine and basaltic liquid on pressure, temperature and composition, *Contrib. Mineral. Petrol.*, *101*, 261–273.

Wagner, T. P., and T. L. Grove (1998), Melt/harzburgite reaction in the petrogenesis of tholeiitic magma from Kilauea volcano, Hawaii, *Contrib. Mineral. Petrol.*, *131*, 1–12.

Walter, M. J., S. C. Kohn, D. Araujo, G. P. Bulanova, C. B. Smith, E. Gaillou, J. Wang, A. Steele, and S. B. Shirey (2011), Deep mantle cycling of oceanic crust: Evidence from diamonds and their mineral inclusions, *Science*, *334*, 54–57.

Walter, M. J., et al. (2008), Primary carbonatite melt from deeply subducted oceanic crust, *Nature*, *454*, 622–625.

Weaver, B. L. (1991), The origin of ocean island basalt end-member compositions: Trace element and isotopic constraints, *Earth Planet. Sci. Lett.*, *104*, 381–397.

Willbold, M., and A. Stracke (2006), Trace element composition of mantle end-members: Implications for recycling of oceanic and upper and lower continental crust, *Geochem. Geophys. Geosyst.*, *7*, Q04004, doi:10.1029/2005GC001005.

Willbold, M., and A. Stracke (2010), Formation of enriched mantle components by recycling of upper and lower continental crust, *Chem. Geol.*, *276*, 188–197.

Wu, F., R. J. Walker, Y. Yang, H. Yuan, and J. Yang (2006), The chemical-temporal evolution of lithospheric mantle underlying the North China Craton, *Geochim. Cosmochim. Acta*, *70*, 5013–5034.

Xiao, Y., H. Zhang, and W. Fan (2008), Origin of clinopyroxene megacrysts in the late Mesozoic and Cenozoic basalts from the North China Craton and their constraints on the magma progress of host rocks: A case of the Junan and Hebi, *Acta Petrol. Sin.*, *24*, 65–76.

Xiao, Y., H. Zhang, W. Fan, J. Ying, J. Zhang, X. Zhao, and B. Su (2010), Evolution of lithospheric mantle beneath the Tan-Lu fault zone, eastern North China Craton: Evidence from petrology and geochemistry of peridotite xenoliths, *Lithos*, *117*, 229–246.

Xu, S., K. Nagao, K. Uto, H. Wakita, S. I. Nakai, and C. Liu (1998), He, Sr and Nd isotopes of mantle-derived xenoliths in volcanic rocks of NE China, *J. Asian Earth Sci.*, *16*, 547–556.

Xu, X., S. Y. O'Reilly, W. L. Griffin, X. Zhou, and X. Huang (1998), The nature of the Cenozoic lithosphere at Nushan, eastern China, in *Mantle dynamics and plate interactions in East Asia*, pp. 167–195 , AGU, Washington, D. C.

Xu, X., S. Y. O'Reilly, W. L. Griffin, and X. Zhou (2003), Enrichment of upper mantle peridotite: Petrological, trace element and isotopic evidence in xenoliths from SE China, *Chem. Geol.*, *198*, 163–188.

Xu, Y., and J. Bodinier (2004), Contrasting enrichments in high-and low-temperature mantle xenoliths from Nushan, Eastern China: Results of a single metasomatic event during lithospheric accretion?, *J. Petrol.*, *45*, 321–341.

Xu, Y., M. A. Menzies, P. Vroon, J. Mercier, and C. Lin (1998), Texture–temperature–geochemistry relationships in the upper mantle as revealed from spinel peridotite xenoliths from Wangqing, NE China, *J. Petrol.*, *39*, 469–493.

Xu, Y., J. Ma, F. A. Frey, M. D. Feigenson, and J. Liu (2005), Role of lithosphere–asthenosphere interaction in the genesis of Quaternary alkali and tholeiitic basalts from Datong, western North China Craton, *Chem. Geol.*, *224*, 247–271.

Xu, Y., H. Zhang, H. Qiu, W. Ge, and F. Wu (2012), Oceanic crust components in continental basalts from Shuangliao, Northeast China: Derived from the mantle transition zone?, *Chem. Geol.*, *328*, 168–184.

Yan, J., and J. Zhao (2008), Cenozoic alkali basalts from Jingpohu, NE China: The role of lithosphere–asthenosphere interaction, *J. Asian Earth Sci.*, *33*, 106–121.

Yang, Y., H. Zhang, Z. Chu, L. Xie, and F. Wu (2010), Combined chemical separation of Lu, Hf, Rb, Sr, Sm and Nd from a single rock digest and precise and accurate isotope determinations of Lu–Hf, Rb–Sr and Sm–Nd isotope systems using Multi-Collector ICP-MS and TIMS, *Int. J. Mass Spectrom.*, *290*, 120–126.

Yaxley, G. M. (2000), Experimental study of the phase and melting relations of homogeneous basalt + peridotite mixtures and implications for the petrogenesis of flood basalts, *Contrib. Mineral. Petrol.*, *139*, 326–338.

Yaxley, G. M., and D. H. Green (1998), Reactions between eclogite and peridotite: Mantle refertilisation by subduction of oceanic crust, *Schweiz. Mineral. Petrogr. Mitt.*, *78*, 243–255.

Yu, S., Y. Xu, X. Huang, J. Ma, W. Ge, H. Zhang, and X. Qin (2009), Hf–Nd isotopic decoupling in continental mantle lithosphere beneath Northeast China: Effects of pervasive mantle metasomatism, *J. Asian Earth Sci.*, *35*, 554–570.

Yu, X., C. A. Lee, L. Chen, and G. Zeng (2015), Magmatic recharge in continental flood basalts: Insights from the Chifeng igneous province in Inner Mongolia, *Geochem. Geophys. Geosyst.*, *16*, 2082–2096, doi:10.1002/2015GC005805.

Zeng, G., L. Chen, S. Hu, X. Xu, and L. Yang (2013), Genesis of Cenozoic low-Ca alkaline basalts in the Nanjing basaltic field, eastern China: The case for mantle xenolith-magma interaction, *Geochem. Geophys. Geosyst.*, *14*, 1660–1677, doi:10.1002/ggge.20127.

Zhang, H. (2005), Transformation of lithospheric mantle through peridotite-melt reaction: A case of Sino-Korean craton, *Earth Planet. Sci. Lett.*, *237*, 768–780.

Zhang, L., D. Prelević, N. Li, R. Mertz-Kraus, and S. Buhre (2016), Variation of olivine composition in the volcanic rocks in the Songliao basin, NE China: Lithosphere control on the origin of the K-rich intraplate mafic lavas, *Lithos*, *262*, 153–168.

Zhang, M., P. Suddaby, R. N. Thompson, M. F. Thirlwall, and M. A. Menzies (1995), Potassic volcanic rocks in NE China: Geochemical constraints on mantle source and magma genesis, *J. Petrol.*, *36*, 1275–1303.

Zhang, M., P. Suddaby, S. Y. O'Reilly, M. Norman, and J. Qiu (2000), Nature of the lithospheric mantle beneath the eastern part of the Central Asian fold belt: Mantle xenolith evidence, *Tectonophysics*, *328*, 131–156.

Zhang, M., J. Yang, J. Sun, F. Wu, and M. Zhang (2012), Juvenile subcontinental lithospheric mantle beneath the eastern part of the Central Asian Orogenic Belt, *Chem. Geol.*, *328*, 109–122.

Zhang, Y., C. Liu, W. Ge, F. Wu, and Z. Chu (2011), Ancient sub-continental lithospheric mantle (SCLM) beneath the eastern part of the Central Asian Orogenic Belt (CAOB): Implications for crust–mantle decoupling, *Lithos*, *126*, 233–247.

Zhao, X. M., H. F. Zhang, X. K. Zhu, W. H. Zhang, Y. H. Yang, and Y. J. Tang (2007), Metasomatism of Mesozoic and Cenozoic lithospheric mantle beneath the North China Craton: Evidence from phlogopite-bearing mantle xenoliths, *Acta Petrol. Sin.*, *23*, 1281–1293.

Zhao, Y., Q. Fan, H. Zou, and N. Li (2014), Geochemistry of Quaternary basaltic lavas from the Nuomin volcanic field, Inner Mongolia: Implications for the origin of potassic volcanic rocks in Northeastern China, *Lithos*, *196–197*, 169–180.

Zou, H., Q. Fan, and Y. Yao (2008), U–Th systematics of dispersed young volcanoes in NE China: Asthenosphere upwelling caused by piling up and upward thickening of stagnant Pacific slab, *Chem. Geol.*, *255*, 134–142.

Zou, H., M. R. Reid, Y. Liu, Y. Yao, X. Xu, and Q. Fan (2003), Constraints on the origin of historic potassic basalts from northeast China by U–Th disequilibrium data, *Chem. Geol.*, *200*, 189–201.

Zhou, Q., F. Y. Wu, Z. Y. Chu, Y. H. Yang, D. Y. Sun, and W. C. Ge (2007), Sr-Nd-Hf-Os isotopic characterizations of the Jiaohe peridotite xenoliths in Jilin province and constraints on the lithospheric mantle age in northeast China, *Acta Petrol. Sin.*, *23*, 1269–1280.

Zhou, Q., F. Y. Wu, Z. Y. Chu, and W. C. Ge (2010), Isotopic compositions of mantle xenoliths and age of the lithospheric mantle in Yitong, Jilin Province. *Acta Petrol. Sin.*, *26*, 1241–1264.